Invited review article

Inter-comparison of extra-tropical cyclone activity in nine reanalysis datasets

CrossMark

Xiaolan L. Wang *, Yang Feng, Rodney Chan, Victor Isaac

Climate Research Division, Science and Technology Branch, Environment and Climate Change Canada, Canada

ABSTRACT

This study inter-compares extratropical cyclone activity in the following nine reanalysis datasets: the ERA-20C Reanalysis (ERA20C), the Twentieth Century Reanalysis, version 2c (20CR), the Japanese 55-year Reanalysis (JRA55), the Modern Era Retrospective-analysis for Research and Applications (MERRA), the NCEP Climate Forecast System Reanalysis (CFSR), the ERA-Interim Reanalysis (ERAint), the ERA40 Reanalysis, the NCEP–NCAR Reanalysis (NCEP1), and the NCEP-DOE Reanalysis (NCEP2). The inter-comparison is based on cyclones identified using an objective cyclone tracking algorithm.

In general, reanalyses of higher horizontal resolutions show higher cyclone counts, with MERRA and 20CR showing the highest and lowest mean counts of all-cyclones, respectively. However, MERRA shows the highest mean intensity (i.e., geostrophic winds) of all-cyclones, and CFSR the lowest, although MERRA and CFSR share a similar horizontal resolution. MERRA is most different from the other datasets, showing many more cyclones of shallow-medium core pressures and much higher counts of cyclones of strong intensity than the others, while CFSR shows many more cyclones of moderate intensity than the others. MERRA cyclones tend to have weaker surface winds but stronger geostrophic winds than the corresponding CFSR cyclones.

The track-to-track agreement between the datasets is better for moderate-deep cyclones than for shallow ones, better in the NH than in the SH, and better in winter than in summer in both hemispheres.

There is more similarity in temporal trends and variability than in specific cyclone counts and intensity, and more similarity in deep-cyclone (core pressure ≤ 980 hPa) statistics than in all-cyclone statistics. In particular, all the four datasets that cover the period from 1958 to 2010 agree well in terms of trend direction and interannual variability in hemispheric counts of deep-cyclones, showing a general increase in both hemispheres over the past half century, although the magnitude of increase varies notably from dataset to dataset. The agreement in trends of deep-cyclone counts is generally better in winter than in summer, and better in the NH than in the SH, with nearly perfect agreement for the counts of NH winter deep-cyclones. However, the nine datasets do not agree well in terms of trend and interannual variability in the mean intensity of deep cyclones, especially in summer and in SH winter.

The temporal homogeneity of cyclone statistics in each dataset was also analyzed. The results show that ERAint, NCEP2, MERRA, ERA40, and CFSR are homogeneous for the NH, and that ERAint and NCEP2 are also homogeneous for the SH. However, large inhomogeneities were found in the other datasets, especially in the earlier period. Most of the identified inhomogeneities coincide with changes in the quantity and/or types of assimilated observations. These inhomogeneities contribute notably to the differences between the datasets, which are larger in the earlier period than in the recent decades. Better trend agreements between these datasets are seen after the inhomogeneities are accounted for. It is critically important to identify and account for temporal inhomogeneities when using these datasets to analyze trends.

Crown Copyright © 2016 Published by Elsevier B.V. This is an open access article under the CC BY-NC-ND license (http://creativecommons.org/licenses/by-nc-nd/4.0/).

Contents

---

* Corresponding author at: Climate Research Division, Science and Technology Branch, Environment and Climate Change Canada, 4905 Dufferin Street, Downsview, ON M3H 5T4, Canada.

E-mail address: Xiaolan.Wang@canada.ca (X.L. Wang).

1. Introduction

A cyclone refers to the center of a closed surface cyclonic circulation, which has counter-clockwise (clockwise) motion of the air in the Northern Hemisphere (Southern Hemisphere). Usually, cyclones outside the tropics are called extra-tropical cyclones, and cyclones that form in the tropics, tropical cyclones. A tropical cyclone can transform into an extratropical cyclone at the end of their tropical existence (usually between 30° and 40°). By a strict definition, a cyclone is called a storm when the wind speed reaches the Storm category on the Beaufort Wind Scale (WMO, 1970), i.e., attains values >24.5 ms^{-1} (Bader et al., 2011). A brief summary of the formalized description, conceptual models describing cyclogenesis, and storm track diagnostic techniques can be found in Bader et al. (2011).

The most obvious impact of cyclones on our society and environment is that cyclones are usually accompanied by adverse weather conditions. They play an important role in determining the local weather and its typical variation, strongly influencing the local precipitation, cloudiness, radiation, and their spatio-temporal variability. Cyclones also represent a primary mechanism for the vertical and horizontal exchange of heat, moisture, and momentum, interacting with the large-scale atmospheric centers of action. Thus, a systematic change in cyclone characteristics (intensity, frequency, lifespan, trajectory) will have substantial impacts on regional climates.

Atmospheric reanalyses use a modern Numerical Weather Prediction (NWP) model to integrate various historical weather/climate observations in a dynamically consistent way, to robustly recover comprehensive climate data records, which cover the entire globe from the Earth's surface to well above the stratosphere. The resulting climate data records are called reanalysis datasets, which have been widely used in a wide range of climate studies and applications. For example, various reanalysis datasets have allowed a large number of studies to systematically assess the climatology, trends, and variability of extra-tropical cyclone activity,

with a number of automatic objective cyclone tracking methods being developed (e.g., Li et al., 2014; Tilinina et al., 2013; Eichler and Gottschalck, 2013a, 2013b; Wang et al., 2013; Raible et al., 2008; Wernli and Schwierz, 2006; Wang et al., 2006; Hanson et al., 2004; Hodges et al., 2003; Gulev et al., 2001; Geng and Sugi, 2001; Simmonds and Keay, 2000; Sinclair, 1994, 1997). Ulbrich et al. (2009) give a comprehensive review of studies of extratropical cyclone climatology and trends using different reanalysis datasets and/or different cyclone tracking methods.

The National Centers for Environmental Prediction (NCEP) of the National Oceanic and Atmospheric Administration (NOAA) of the United States is the pioneer in reanalysis, producing the very first two reanalysis datasets — the NCEP–NCAR reanalysis (NCEP1) (Kalnay et al., 1996; Kistler et al., 2001) and NCEP-Department of Energy reanalysis (NCEP2) (Kanamitsu et al., 2002), as well as the first coupled reanalysis dataset — the NCEP Climate Forecast System Reanalysis (CFSR) (Saha et al., 2010). The European Centre for Medium-Range Weather Forecasts (ECMWF) is the other major player in this field and has produced four reanalysis datasets: the ERA-15 reanalysis (Gibson et al., 1997), the ERA40 Reanalysis (Uppala et al., 2005), the ERA-Interim Reanalysis (ERAint) (Dee et al., 2011), and the most recent ERA-20C Reanalysis for the Twentieth Century (ERA20C) (Poli et al., 2013). Other four commonly-used reanalysis datasets include the NOAA Twentieth Century Reanalysis (20CR) (Compo et al., 2011), the Modern Era Retrospective-analysis for Research and Applications (MERRA) of the National Aeronautics and Space Administration (NASA) of the United States (Rienecker et al., 2011), the Japanese JRA-55 Reanalysis (JRA55) (Kobayashi et al., 2015; Ebita et al., 2011), and the Japanese JRA-25 Reanalysis (JRA25) (Onogi et al., 2007).

Among the existing datasets, the ERA20C and JRA55 datasets were completed most recently. Thus, there is limited publications of cyclone activity studies using these two datasets. The other datasets have been used to characterize the climatology, trends, and variability of extra-

Table 1

The nine global reanalysis datasets analyzed in this study and their resolutions and data periods. Model resolution is represented by the number of vertical levels (L#) and their spectral truncation (T#) or horizontal latitude–longitude grid for non-spectral models. The output grid refers to the horizontal grid (Lat#, Lon#) on which model output is available. The resolution (in km) of global spectral models is estimated using $L_2 \sim 20/n$, where n is the # in T# (Laprise, 1992).

Reanalysis	Period covered	Model resolution	Output grid (Lat# × Lon#)
The ERA-20C reanalysis (ERA20C); Poli et al. (2013)	1900–2010	L91, T159 (~126 km)	181 × 360
The NOAA Twentieth Century Reanalysis, version v2c (20CR); Compo et al. (2011); http://rda.ucar.edu/datasets/ds131.2/	1831–2011	L28, T62 (~323 km)	90 × 180
The Japanese 55-year Re-Analysis (JRA55); Kobayashi et al. (2015) and Ebita et al. (2011)	1958–2012	L60, T319 (~63 km)	144 × 288
The NASA Modern Era Retrospective-analysis for Research and Applications (MERRA); Rienecker et al. (2011)	1979–2012	L72, 0.5° × (2°/3) (~28 km)	270 × 720
The NCEP Climate Forecast System Reanalysis (CFSR); Saha et al. (2010)	1979–2009	L64, T382 (~52 km)	360 × 720
The ECMWF Interim Reanalysis (ERAint); Dee et al. (2011)	1979–2010	L60, T255 (~78 km)	240 × 480
The ECMWF ERA40 Reanalysis (ERA40); Uppala et al. (2005)	1958–2001	L60, T159 (~126 km)	72 × 144
The NCEP-Department of Energy reanalysis (NCEP2); Kanamitsu et al. (2002)	1979–2008	L28, T62 (~323 km)	72 × 144
The NCEP–NCAR reanalysis (NCEP1); Kalnay et al. (1996)	1948–2010	L28, T62 (~323 km)	72 × 144

Table 2

Significant (at the 5% level) changepoints identified in the time series of the consecutive seasonal all-cyclone statistics averaged over the indicated region. A blank entry indicates that the corresponding time series is homogeneous at the 5% level. Note that ERAint and NCEP2 are not listed below because they were found to be homogeneous over both Northern and Southern Hemispheres, and that 20CR is listed in a continued part of this table. The dates of changepoints are in YYYYSS format, standing for year and season, with SS = 01,02,03,04 corresponding to JFM, AMJ, JAS, and OND, respectively. Here, "Yes" indicates that the changepoint is significant even without metadata support (a very big inhomogeneity); "YifD" indicates that it is significant only if it has metadata support; and "?" indicates that it may or may not be significant, because its test statistic lies within the 95% uncertainty range of the corresponding critical values (a subjective judgment is needed in this case; see Wang, 2008a for details).

Data set	Region	Cyclone counts		Cyclone intensity	
		Type	Date	Type	Date
ERA20C	Arctic	1 Yes	191404		
	NH	1 Yes	191904	1 Yes	190404
				1 Yes	191904
				1 Yes	194202
				1 Yes	195104
	NHland			1 Yes	190404
				1 Yes	194202
				1 Yes	195104
	NHsea	1 Yes	191904	1?	190404
				1 Yes	191904
				1 Yes	194202
	SH	1?	191004	1 Yes	191404
		1 Yes	191404	0 Yes	200504
		1 Yes	191904		
		1 Yes	194202		
		1 Yes	194703		
		1 Yes	197804		
	SHland			0 Yes	200504
	SHsea	1?	191004	1 Yes	191404
		1 Yes	191404	0 Yes	200504
		1 Yes	191904		
		1 Yes	194202		
		1 Yes	194703		
		1 Yes	197804		
JRA55	Arctic				
	NH			0 Yes	199704
	NHland			0 YifD	199704
	NHsea			0 YifD	199704
	SH	0 YifD	197804	0 Yes	199704
		1 Yes	198104		
	SHland				
	SHsea	0 Yes	197804	0 Yes	199704
		1 Yes	198104		
20CR	Arctic	0 Yes	187004	0 Yes	187004
		0 Yes	188103	0 Yes	188103
		0 YifD	190004	1?	189304
		0 Yes	194203	0 Yes	190004
		0 Yes	194804	0 Yes	190802
				0 Yes	192004
				0 YifD	192504
				0 Yes	193004
				0 Yes	193303
				0 Yes	194203
				0 Yes	194804
	NH	1 Yes	188201	0 Yes	187004
		1 Yes	188604	0 Yes	190004
		0 Yes	190004	0 Yes	193004
		0 Yes	194504		
	NHland	1 Yes	188201	0 Yes	187004
		1?	188604	0 Yes	190004
		0 Yes	194504	0 Yes	192004
				0 Yes	193004
	NHsea	1 Yes	184203	0 Yes	187004
		1 Yes	188201	0 YifD	190004
		1 Yes	188604	0 Yes	193004
		0 Yes	194004		
		0 Yes	194504		

Data set	Region	Cyclone counts		Cyclone intensity	
		Type	Date	Type	Date
MERRA	Arctic				
	NH				
	NHland				
	NHsea				
	SH	0 YifD	198702	0 Yes	200602
		0 YifD	199804		
	SHland				
	SHsea	0?	198702		
		0 Yes	199804	0 Yes	200602
ERA40	Arctic				
	NH				
	NHland				
	NHsea				
	SH	0 Yes	197204	0 Yes	197404
		0 YifD	197804	0 Yes	197601
	SHland				
	SHsea	0 Yes	197204	0 Yes	197404
		0 Yes	197804	0 Yes	197601
CFSR	Arctic				
	NH				
	NHland				
	NHsea				
	SH	0 YifD	199204	0 YifD	199204
	SHland				
	SHsea	0 Yes	199204	0 YifD	199204
NCEP1	Arctic				
	NH	0 YifD	195604	0 Yes	195604
	NHland	0 YifD	195604	0 YifD	195604
	NHsea	0 Yes	195604	0 YifD	195604
	SH	0 YifD	197804	0 YifD	195604
		0 Yes	199804	0 Yes	197804
				0 YifD	199804
	SHland			0 Yes	195604
				0 Yes	199804
	SHsea	0 YifD	197804	0?	195604
		0 Yes	199804	0 YifD	197804
				0 YifD	199804
20CR	SH	1 Yes	185002	1 Yes	185402
		1 Yes	185402	0 Yes	195102
		0 Yes	188301	0 Yes	200503
		0 Yes	188603		
		0 Yes	195102		
		0 Yes	197804		
		0 Yes	198504		
		0 Yes	200503		
	SHland	1 Yes	185002	1 Yes	185002
		0 Yes	195102	0 Yes	195102
		0 Yes	198504		
		0 Yes	200503		
	SHsea	1 Yes	185002	1 Yes	185402
		1 Yes	185402	0 Yes	195102
		0 Yes	188301	0 Yes	200503
		0 Yes	188603		
		1 Yes	195102		
		0 Yes	197804		
		0 YifD	198504		
		0 YifD	200503		

tropical cyclone activity in a number of studies. These studies have reported changes in extra-tropical cyclone activity in several regions (Ulbrich et al., 2009; Wang et al., 2013; Wang et al., 2006; Gulev et al., 2001; among others). In particular, the IPCC AR5 report (Hartmann et al., 2013) stated that "studies using reanalyses continue to support a northward and eastward shift in the Atlantic cyclone activity during

the last 60 years with both more frequent and more intense wintertime cyclones in the high-latitude Atlantic and fewer in the mid-latitude Atlantic."

However, the cyclone trend results can be dependent on the choice of the reanalysis dataset and of the tracking method used, and on the choice of the specific domain and period to analyze trends (Ulbrich et al., 2009; Neu et al., 2013; Raible et al., 2008). For example, Wang et al. (2006) reported that NCEP1 and ERA40 are in reasonably good agreement with each other in terms of the climatology and trends of cyclones over northern Europe and eastern North America, while ERA40 shows systematically stronger cyclone activity over the boreal extratropical oceans than does NCEP1. Trigo (2006) reported that both ERA40 and NCEP1 show similar trends in the counts of cyclones over Europe (an increase over Northern Europe, matched with a decrease in Central Europe), while trends in other regions are more dependent

on the underlying dataset. Lehmann et al. (2011) show an increase in intensity and number of extreme Atlantic cyclones, while Gulev et al. (2001) show opposite trends in eastern Pacific and North America. More examples and details can be found in the comprehensive review by Ulbrich et al. (2009).

Discrepancies between two reanalysis datasets can also arise from differences in the horizontal resolution, the dynamics and the parametrization implemented in the NWP model used to produce the reanalyses (Ulbrich et al., 2009). Previous studies (e.g., Wang et al., 2013; Wang et al., 2006) also show that changes over time in the types and spatial/temporal densities of observational data available for assimilation in the reanalyses can cause temporal inhomogeneities in the reanalysis data, which could affect the assessment of climate trends and variability using the reanalysis data. As different reanalysis products assimilated different observations, some are less prone or even immune to issues

Table 3
Same as in Table 2 but for deep-cyclones. Note that ERAint, NCEP2, and MERRA are not listed below because they were found to be homogeneous over both hemispheres.

Data set	Region	Cyclone counts		Cyclone intensity	
		Type	Date	Type	Date
ERA20C	Arctic				
	NH	1 Yes	191504		
		0 YifD	194203		
		0 Yes	200801		
	NHland	1 Yes	191504		
		0 YifD	194203		
		0 YifD	199504		
		0 Yes	200801		
	NHsea	1 Yes	191504		
		0 YifD	194203		
		0 YifD	200801		
	SH			0 YifD	200504
	SHland			0 YifD	200504
	SHsea			0 YifD	200504
20CR	Arctic	1 Yes	183602	1 Yes	183602
		0 Yes	187004	0 Yes	187004
		0 Yes	193303	0 Yes	193303
				0 YifD	194203
				0 YifD	194804
	NH	1 Yes	183602	1?	183602
		0 Yes	187004		
		0 Yes	193004		
	NHland	1 Yes	183602	1?	183602
		0 Yes	187004		
		0 Yes	193004		
	NHsea	1 Yes	183602	1 No	183602
		0 Yes	187004		
		0 Yes	193004		
	SH	1 Yes	183602	1 Yes	183602
		1 Yes	185402	1 Yes	185402
		0 Yes	188301	1 Yes	188301
		0 Yes	188603	1 Yes	188603
		1 Yes	191204	1 Yes	191204
		0 Yes	192004	0 Yes	192004
		0 Yes	195102	0 Yes	195102
		0 YifD	197804	0 YifD	197804
	SHland	1 Yes	183602	1 Yes	183602
		1 Yes	185402	1 Yes	185402
		0 Yes	188301	1 Yes	188301
		0 Yes	188603	1 Yes	188603
		1 Yes	191204	1 Yes	191204
		0 YifD	192004	0 Yes	192004
				0 Yes	195102
				0 YifD	197804
	SHsea	1 Yes	183602	1 Yes	183602
		1 Yes	185402	1?	185402
		0 Yes	188301	1 Yes	188301
		0 Yes	188603	1 Yes	188603
		1 Yes	191204	1 Yes	191204
		0 Yes	192004	0 Yes	192004
		0 Yes	195102	0 Yes	195102
		0 YifD	197804	0 YifD	197804

Data set	Region	Cyclone counts		Cyclone intensity	
		Type	Date	Type	Date
JRA55	Arctic				
	NH			0 YifD	197204
		0 Yes	199704	0 YifD	199704
	NHland			0 No	197204
				0?	199704
	NHsea			0 YifD	197204
		0 Yes	199704	0 YifD	199704
	SH	0 Yes	197204		
	SHland	0 Yes	197204		
	SHsea	0 Yes	197204		
CFSR	Arctic				
	NH				
	NHland				
	NHsea				
	SH	0 YifD	199204	0 Yes	199204
	SHland			0 YifD	199204
	SHsea	0 YifD	199204	0 Yes	199204
ERA40	Arctic				
	NH				
	NHland				
	NHsea				
	SH			0 Yes	197404
				0 YifD	197601
	SHland			0 Yes	197404
				0 YifD	197804
	SHsea			0 Yes	197404
NCEP1	Arctic				
	NH	0 YifD	200801	1 Yes	195304
	NHland	0 YifD	200801	1 Yes	195304
	NHsea	0 YifD	200801		
	SH	0 Yes	195604	0 Yes	195604
				0 YifD	197804
				0 YifD	199804
	SHland	0 YifD	195604	0 Yes	195604
				0 Yes	199504
	SHsea	0 Yes	195604	0 YifD	195604
				0 YifD	197804
				0 YifD	199804

affecting others. For example, 20CR and ERA20C did not assimilate upper air and satellite data and thus should not be affected by changes/issues in these types of data. Therefore, it is necessary to inter-compare the existing reanalysis datasets in different terms, including how they represent the climatology, trends, and variability of cyclone activities.

A few recent studies on the inter-comparison of extratropical cyclone activity in different reanalysis datasets on the global or hemispheric or regional scales have been published. In particular, six studies that intercompare multiple reanalysis datasets in terms of extratropical cyclone activity on the global or hemispheric scales were published after the comprehensive review of Ulbrich et al. (2009). A brief review of these recent global or hemispheric scale studies follow next (we exclude regional studies from our focus here).

On the global scale, Hodges et al. (2011) focused on comparing the number and characteristics of extratropical cyclones in the ERAint, MERRA, CFSR, and the older JRA25 reanalysis datasets for the period 1989–2009. They reported that newer, higher resolution reanalyses inter-compare much better than older reanalysis datasets, with the greatest improvement being seen in the Southern Hemisphere (SH), and that the inter-comparison for cyclone count and spatial distribution is very good, while the inter-comparison of maximum cyclone intensity is poor, especially when other reanalyses are compared to MERRA. They also mentioned an inhomogeneity related to the increase in assimilated data quality with the introduction of satellite data which was especially prevalent in the SH. Allen et al. (2010) analyzed the representation of explosive cyclones in the ERA40, ERAint, NCEP1, NCEP2, and JRA25 datasets for the time period 1979–2008. They found strong agreement and strong positive correlation coefficients between all the five datasets in the Northern Hemisphere (NH), with poor agreement and small correlation coefficients being seen in the SH. Wang et al. (2013) compared 20CR with NCEP1 on the global scale for the period 1951–2010 and found that the 20CR ensemble-averaged statistics of extratropical cyclones generally agree well with statistics from the NCEP1, although 20CR shows somewhat weaker cyclone activity over land and stronger activity over oceans.

Focusing on the NH, Tilinina et al. (2013) compared the number and characteristics of cyclones in six different classes in the NCEP1, NCEP2, JRA25, ERAint, and MERRA datasets. They reported that the number of cyclones increases with the resolution of the reanalyses, that MERRA shows the highest number of cyclones as well as a significantly higher number of very deep (<930 hPa) cyclones, and that MERRA shows stronger deepening rates as well as shorter lifetimes of cyclones. In terms of trends, they found that NCEP2 and ERAint show significant positive trends of 1–2% per decade in the total number of cyclones, but that this increase is almost entirely seen in shallow (>1000 hPa) or moderate (980–1000 hPa) cyclones. They also found that in most reanalysis datasets the number of very deep cyclones increases in the North Atlantic until 1990 before decreasing until the present, while the number of cyclones in the North Pacific increases until 2000 before decreasing to the present. Large inhomogeneities associated with the sharp increase in assimilated data coinciding with the availability of satellite data were found to be most noticeable in the SH (Tilinina et al., 2013). Akperov and Mokhov (2010) also intercompared NCEP1, ERA40, and ERAint in terms of NH extratropical cyclones. They found that NCEP1 and ERA40 include fewer small radii cyclones than does ERAint due to their lower horizontal resolution, while ERAint includes deeper cyclones. Chang and Yau (2016) intercompared the ERA20C, 20CR, JRA55, ERAint, NCEP1, and ERA40 in terms of the Northern Hemisphere winter storm track trend since 1959. Their comparison with trends derived from rawinsonde observations suggest that the NCEP1 trends are significantly biased high, while the ERA40 and JRA55 are much less biased but still too high, and that the 20CR trends are most consistent with observations but may
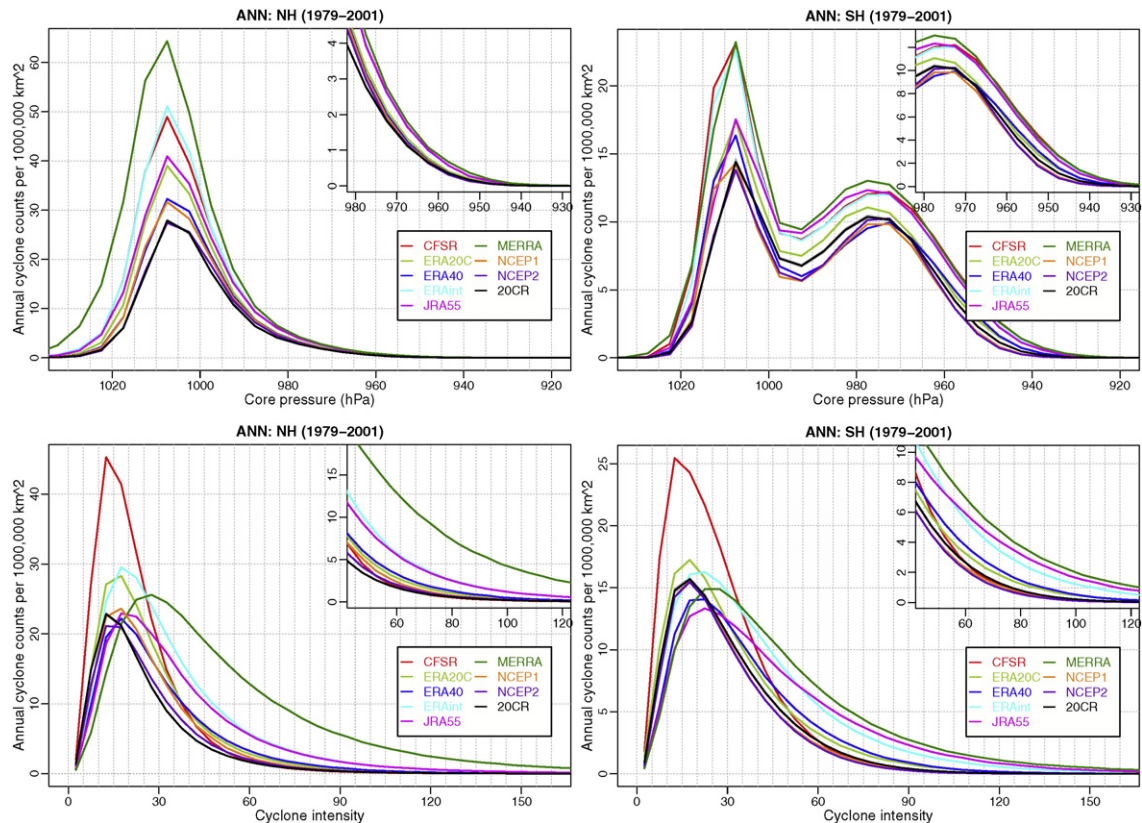

Fig. 1. Distribution of annual cyclone counts over the core pressure (upper panels) and over the intensity (lower panels) for the common period 1979–2001 of the nine reanalysis datasets, for the northern and southern hemispheres (NH and SH) separately. Here, cyclone intensity is the local Laplacian of pressure (unit: 10^{-5} hPa km^{-2}).
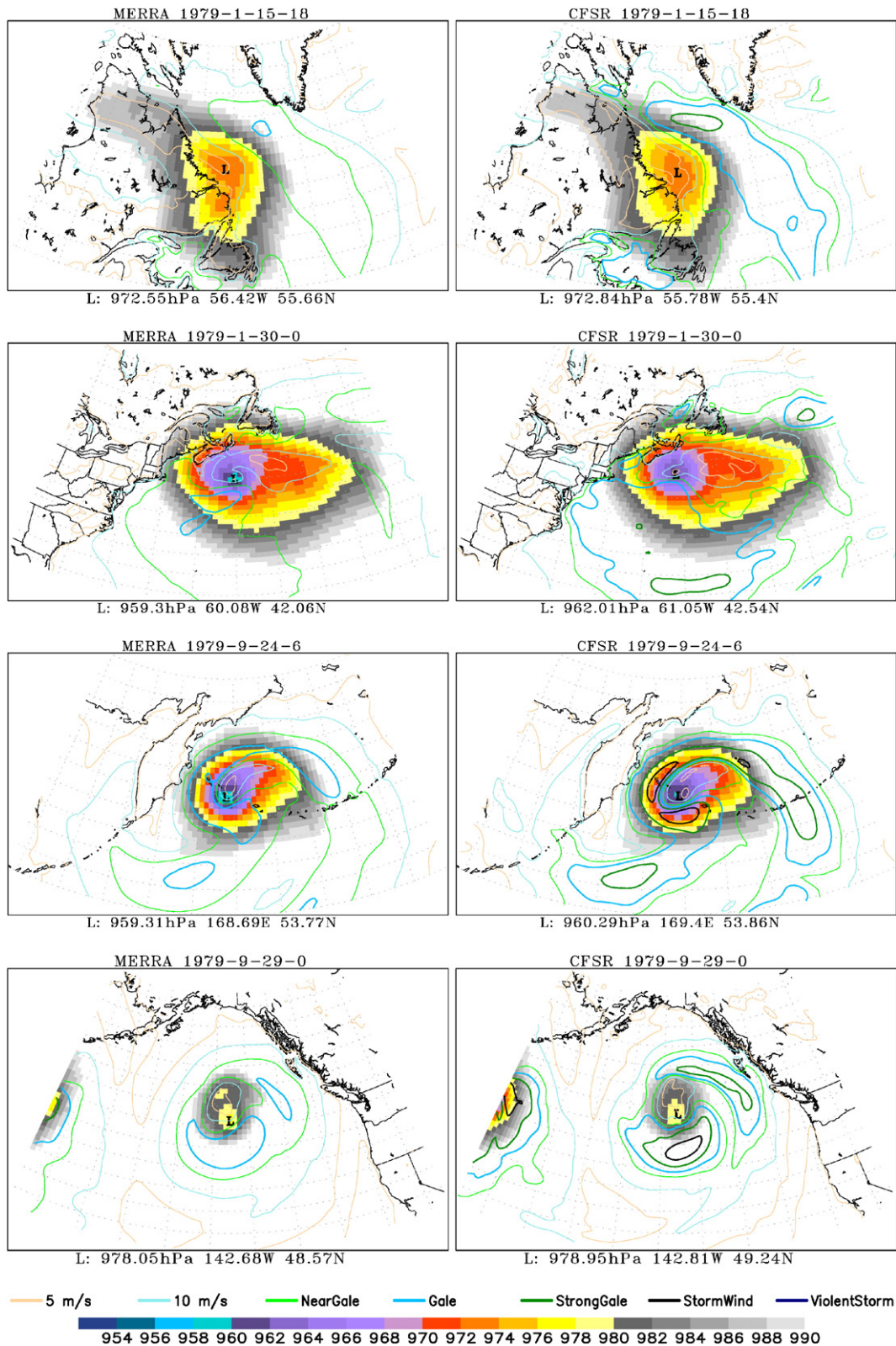
Fig. 2. Maps of MSLP (shadings; unit: hPa) and surface winds (contours) around a few selected pairs of best-match cyclones in the MERRA and CFSR datasets. The cyclone center is marked with L; the core pressure and center location (latitude, longitude) are given in the bottom of each panel, and the dates (year–month–day–hour) on the top.

exhibit slight biases of opposite signs. Note that temporal homogeneity was not assessed or accounted for in Chang and Yau (2016).

In order to systematically study the climatology, trends, and variability of extra-tropical cyclone activity using a gridded dataset (such as a reanalysis dataset), a number of automatic objective cyclone tracking methods have been developed. Recently, a community effort (Neu et al., 2013) of the inter-comparison of mid-latitude storm diagnostics (IMILAST) project of the World Climate Research Program focused on the inter-comparison of cyclone tracking methods. It inter-compared 15 methods using the same input dataset (ERAint) in order to assess

the similarities and differences in the resulting cyclone characteristics. The results show that the spatial patterns of geographical distribution and interannual variability of cyclones are qualitatively consistent across the methods, while quantitative differences in the total numbers of extratropical cyclones are relatively large in both hemispheres. The results also show that "consistency across the methods is generally higher for deep (or strong) cyclones than for shallow ones", and that the geographical linear trend patterns are qualitatively consistent, with regions of strong trends showing a good agreement (at least in sign) over most methods.

In contrast to Neu et al. (2013), the present study focused on the inter-comparison of different reanalysis datasets in terms of cyclone activity, by applying the same cyclone tracking algorithm to each and every dataset. The focus of the inter-comparison is on the climatology, trends, and variability of extratropical cyclone activity in the nine global reanalysis datasets listed in Table 1. The data and methodology used in this study are described in Section 2. The temporal homogeneity analysis of cyclone statistics in the nine reanalysis datasets are described in Section 3. The intercomparison of cyclone activities are presented and discussed in Section 4. Finally, conclusions are drawn in Section 5 to complete this study.

2. Data and methodology

A systematic study of cyclone activity on the global and/or regional scales is usually based on applying an objective cyclone tracking algorithm to the fields of a selected atmospheric variable, such as the mean sea level pressure (MSLP), geopotential height and cyclonic vorticity at different levels (see Neu et al., 2013 for example). Previous studies have found that the use the unfiltered MSLP or geopotential height fields generally emphasizes the large spatial scale features and is strongly influenced by large spatial scale (such as Icelandic low) and strong background flows, while the use of vorticity fields tends to identify smaller spatial scale features, although vorticity fields do not depend as strongly on the background flow (Hoskins and Hodges, 2002). There have been attempts to diminish the influence of background flows by removing an estimate of the background flow (e.g., Hoskins and Hodges, 2002; Anderson et al., 2003; Hodges et al., 2003, among others), or by filtering the identified cyclones with a threshold of cyclone lifespan and of travel distance (e.g., Neu et al., 2013; Wang et al., 2006, 2013; Hodges et al., 2011; among others).

In order to focus on the large scale features of cyclone activity, we applied a cyclone tracking algorithm to the unfiltered MSLP fields in this study. To diminish the background influence, we excluded the cyclones that last for less than four 6-hourly time-steps and travel <500 km in straight-line distance during their lifetime. Considering that the results of tracking MSLP fields may be sensitive to how surface pressure is extrapolated to MSLP and the representation of the orography in the model (Hoskins and Hodges, 2002), we also excluded cyclones in elevated areas, namely, areas of elevation ≥1500 m.

Next, we describe the datasets and the cyclone tracking algorithm used in this study in the two subsections below.

2.1. Data

In this study, we analyzed the MSLP fields taken from the following nine global reanalysis datasets: ERA20C, 20CR, JRA55, MERRA, CFSR, ERAint, ERA40, NCEP2, and NCEP1. Their full names, horizontal resolutions, data periods, and references are detailed in Table 1. Among these, ERA20C and 20CR are the only two reanalysis datasets that assimilated observations of surface pressure only (ERA20C also assimilated surface marine winds), and that span the entire twentieth century. All the other datasets assimilated also other observations, including upper air (radiosonde) and satellite observations. In this section, we provide a very brief description of each reanalysis dataset.

ERA20C used a coupled Atmosphere/Land-surface/Ocean-waves model, at a T159 horizontal resolution (approximately 125 km), and a four-dimensional variational (4D-Var) analysis scheme, with variational bias correction of surface pressure observations (Poli et al., 2013). The spatio-temporal evolution of background errors was provided by a 10-member ensemble produced a priori (Poli et al., 2013). ERA20C was produced employing 22 parallel 5-year streams (Jan 1900–Dec 1904, Jan 1905–Dec 1909, …), with a spin-up period of one year (12 months) prior to each production stream.

20CR is a 56-member ensemble of surface-based reanalyses; each and every one of the 56 members was analyzed in this study. It used an Ensemble Kalman Filter data assimilation method, with background first-guess fields being supplied by an ensemble of NWP model forecasts (Compo et al., 2011). The NWP model is a coupled atmosphere–land model (the NCEP Global Forecast System), at a T62 horizontal resolution (see Compo et al., 2011 and references therein for a complete description). 20CR was produced employing 5-year parallel streams (Jan 1871–Dec 1875, Jan 1876–Dec 1880, …), with a spin-up period of 14 months prior to each production stream. In this study we used the 20CR version 2c (v2c) ensemble (http://rda.ucar.edu/datasets/ds131.2/).

JRA55 is based on the TL319 resolution version of the Japanese Meteorological Agency (JMA) operational data assimilation system as of December 2009. The atmospheric component is an incremental 4D-Var system, with analysis increments being produced with the T106 resolution model; the JMA spectral model at TL319 resolution as of December 2009 was used to generate the background and atmospheric forcing fields (Kobayashi et al., in press). JRA55 was originally produced in two streams: 1958–1980 and 1981–2012; but recalculations to correct some technical problems were done for the following three periods: Jan–Jun 1958, Dec 1974–Aug 1980 and Jun 1987–Sep 1992 (Kobayashi et al., in press).

MERRA is based on the Goddard Earth Observing System Data Assimilation System Version 5 (GEOS-5, an atmospheric general circulation model), at the grid of 1/2° latitude × 2/3° longitude (Rienecker et al., 2011). It used a three-dimensional variational (3D-Var) analysis system, with an incremental analysis update procedure. It was produced in three separate streams (1979–1992, 1993–2000, 2001–present), each spun up in two stages: a 2-yr analysis at 2° × 2.5° and then a 1-yr analysis on the MERRA grid (Rienecker et al., 2011).

The CFSR atmospheric analysis is made at T382 horizontal resolution, using a coupled 9-h guess forecast. The atmospheric analysis system and the input data are nearly the same as those used in MERRA; the models used for the land, ocean and sea ice analysis are detailed in Saha et al., (2010). CFSR was produced in six parallel streams (ending December of 1986, 1989, 1994, 1999, 2005, and 2009, respectively), with a 1-yr spin-up period prior to each stream.

ERAint is based on the ECMWF IFS (Integrated Forecast System) release Cy31r2, the model used for operational forecasting at ECMWF from 12 Dec 2006 to 5 Jun 2007, at T255 horizontal resolution. It was produced with a sequential 4D-Var data assimilation system, advancing forward in time using 12-hourly analysis cycles (Dee et al., 2011).

ERA40 is based on the ECMWF IFS cycle 23r4, the model operational from June 2001 to January 2002, at T159 horizontal resolution, though with some modifications. It was produced using a 4D-Var assimilation system with a six-hour assimilation period, in three streams: 1957–1972, 1972–1988, 1989–2002 (Uppala et a., 2005).

Both NCEP1 and NCEP2 are based on the NCEP global spectral model at T62 horizontal resolution, using a 3D-Var analysis system. However, the NCEP1 reanalyses were affected by three human errors made in the assimilation (Kistler et al., 2001): (1) During 1974–1994, snow cover corresponding to 1973 was used every year by mistake. (2) The use of a different convention for longitude led to a shift of 180° in the use of the PABOs (Australian estimates of the sea level pressure) data for 1979–1992. (3) The forecast model had a formulation of the horizontal moisture diffusion that led to unreasonable snowfall over high-latitude valleys in the winter. These three human errors were corrected in the NCEP2 reanalyses.

Table 4a

The counts of cyclone tracks in the NH (20°N–90°N) and SH (20°S–90°S) and the track agreement between the indicated pair of datasets over the common period 1979–2001. The track agreement is expressed in percentage of best-match tracks, relative to the lower count of tracks in the pair of datasets in question. For 20CR, the counts and percentages are the ensemble-averaged counts and percentages. The numbers in the first row are the annual counts of cyclone tracks in the NH. The numbers in the first column are the annual counts of cyclone tracks in the SH. The upper-right and lower-left triangles in each table show the track agreement for the NH and SH. The two highest percentages in each triangle are shown in bold, and the two lowest in italic.

A. Annual	SH	CFSR	ERA20C	ERA40	ERAint	JRA55	MERRA	NCEP1	NCEP2	20CR
NH		3387	2697	2375	3526	3293	5219	2221	1965	1762.9
CFSR	2603		44.8	46.9	43.2	40.5	37.3	43.2	45.6	36.6
ERA20C	2020	11.8		47.7	49.0	44.2	38.8	42.0	45.2	37.1
ERA40	1929	40.9	12.0		**51.4**	48.8	42.0	46.9	50.8	39.3
ERAint	2466	**46.8**	13.5	**46.2**		45.7	39.4	42.2	45.0	*35.6*
JRA55	2423	30.0	10.5	32.4	34.7		40.3	41.8	44.7	36.1
MERRA	2890	36.9	*9.8*	35.6	41.0	28.7		36.4	39	*29.7*
NCEP1	1629	21.0	11.0	26.4	21.7	20.5	19.4		**60.8**	39.7
NCEP2	1587	19.7	10.3	24.9	20.6	19.4	18.8	41.2		39.2
20CR	1693.9	12.1	*8.6*	13.2	12.4	11.6	10.2	12.4	12.0	

As shown in Table 1, the output grid also varies from one reanalysis dataset to another. In general, higher model resolutions correspond to higher output grid resolutions. We interpolated each of these datasets to a 50 × 50 km version of the NSIDC EASE-grid (the Equal Area SSM/I Earth Grid; Armstrong and Brodzik, 1995) over the Northern and Southern Hemispheres, separately, prior to tracking cyclones. The interpolation is based on Cressman weights (as originally designed in the FORTRAN codes developed by Dr. Mark Serreze).

2.2. Cyclone tracking algorithm

The results of the IMILAST method-intercomparison study (Neu et al., 2013) show that the tracking method of Wang et al. (2006), which is a modified version of the method developed by Serreze (1995) (see also Serreze et al., 1997), compares very well with other methods in the IMILAST comparison (see Tables 2–3 of Neu et al., 2013). The tracking method we used in this study is the same as in Wang et al. (2013), which is a modified version of the method of Wang et al. (2006). For each time step, a grid-point in the 50-km EASE grid is identified as a cyclone center if it has the minimum pressure value over a 11×11 array of grid-points and if the minimum pressure is at least a 0.1 hPa lower than the surrounding grid-point values. When adjacent grid-points with identical pressure values are found, the cyclone center is defined as the grid-point with the largest local Laplacian of MSLP. The tracking algorithm uses a nearest neighbour analysis of the positions of systems between time steps (e.g., from 12:00 Z to 18:00 Z), with a maximum distance-threshold of 1000 km between candidate pairings. To identify cyclone intensity, we use the four pressure differences over a 50, 100, 150, and 200 km distance from the cyclone center, respectively, to compute the local maximum Laplacian of MSLP (Wang et al., 2013).

We applied this automatic cyclone tracking algorithm to the 6-hourly MSLP fields on a 50-km EASE grid over the NH and SH, separately, and for each dataset, including each of the 56 members of the 20CR (v2c) ensemble (http://rda.ucar.edu/datasets/ds131.2/). The 20CR ensemble-averaged cyclone statistics are analyzed and compared with those of the other eight reanalysis datasets.

We used both the local Laplacian of pressure (MSLP) and cyclone center/core pressure to measure cyclone intensity. However, in this paper cyclone intensity refers to the local Laplacian of MSLP, unless specified otherwise.

As in Wang et al. (2006), in this study, a cyclone refers to a single low pressure center identified at a specific grid-point and time; while a cyclone track consists of several cyclones that are present at a series of adjacent grid-points and time steps in sequence. Also, deep-cyclones refer to cyclones of core pressure of 980 hPa or lower, while all-cyclones refer to all the identified cyclones (which last for four 6-hourly time-steps or more and travel at least 500 km in straight-line distance during their lifetime).

The NH (SH) extra-tropics is defined as 20°N–90°N (20°S–90°S). All cyclones that occur in these regions are included in the analysis; some of them might have a tropical origin. The analyses were carried out for each season, separately, with the four seasons being defined as JFM (January–February–March), AMJ (April–May–June), JAS (July–August–September), and OND (October–November–December).

3. Temporal homogeneity analysis and results

Reanalysis datasets are prone to bias as they inherit issues from observation systems they assimilate. They are also prone to temporal inhomogeneities of their own as a changing quantity of assimilated

Table 4b

The counts of cyclone tracks in the NH (20°N–90°N) and the track agreement between the indicated pair of datasets over the common period 1979–2001. The track agreement is expressed in percentage of best-match tracks, relative to the lower count of tracks in the pair of datasets in question. For 20CR, the counts and percentages are the ensemble-averaged counts and percentages. The numbers in the first row are the JFM counts of cyclone tracks in the NH. The numbers in the first column are the JAS counts of cyclone tracks in the NH. The upper-right and lower-left triangles in each table show the track agreement for the JFM and JAS seasons in the NH . The two highest percentages in each triangle are shown in bold, and the two lowest in italic.

B. NH	JAS	CFSR	ERA20C	ERA40	ERAint	JRA55	MERRA	NCEP1	NCEP2	20CR
JFM		798	623	536	795	749	1282	531	461	424.5
CFSR	904		50.0	52.9	46.1	45.3	38.4	45.6	49.5	40.9
ERA20C	711	38.9		54.4	54.6	50.2	42.7	44.5	49.6	41.1
ERA40	645	40.7	40.4		**57.2**	55.0	45.6	49.2	55.5	43.6
ERAint	970	38.8	42.3	44.9		50.5	42.0	44.3	49.0	39.8
JRA55	884	35.6	37.9	41.9	40.0		42.4	44.5	48.9	40.0
MERRA	1327	34.5	34.7	37.5	35.4	37.7		*37.5*	41.2	*32.0*
NCEP1	550	40.3	38.5	44.6	39.7	38.8	35.7		**64.1**	44.0
NCEP2	511	40.2	39.1	**45.5**	39.9	39.5	36.0	**56.6**		43.6
20CR	449	31.2	31.5	33.9	*30.7*	31.2	*26.9*	34.6	33.5	

Table 4c
The counts of cyclone tracks in the SH (20°S–90°S) and the track agreement between the indicated pair of datasets over the common period 1979–2001. The track agreement is expressed in percentage of best-match tracks, relative to the lower count of tracks in the pair of datasets in question. For 20CR, the counts and percentages are the ensemble-averaged counts and percentages. The numbers in the first row are the JFM counts of cyclone tracks in the SH. The numbers in the first column are the JAS counts of cyclone tracks in the SH. The upper-right and lower-left triangles in each table show the track agreement for the JFM and JAS seasons in the SH. The two highest percentages in each triangle are shown in bold, and the two lowest in italic.

C. SH	JAS	CFSR	ERA20C	ERA40	ERAint	JRA55	MERRA	NCEP1	NCEP2	20CR
JFM		669	494	495	635	591	721	406	390	415.3
CFSR	626		12.9	37.1	41.7	33.0	33.7	21.0	20.1	12.8
ERA20C	505	11.1		12.5	14.8	11.6	*11.0*	12.4	11.8	*9.5*
ERA40	457	45.5	11.7		**42.3**	34.2	33.7	27.0	25.7	13.8
ERAint	585	**52.3**	12.4	**50.8**		38.4	37.3	22.4	21.4	13.2
JRA55	610	26.5	9.6	30.9	32.1		32.0	20.8	20.7	13.1
MERRA	708	39.6	*8.7*	38.5	45.0	25.2		20.4	20.5	11.2
NCEP1	406	20.6	9.8	25.6	21.1	19.5	18.6		**42.2**	13.1
NCEP2	399	18.8	9.4	23.8	19.7	17.9	17.8	40.0		12.9
20CR	421.8	12.0	*8.1*	13.3	12.3	10.9	9.8	12.0	11.5	

observations can greatly affect output quality, especially in regions where observation networks were sparse such as the SH (Allen et al., 2010; Bromwich et al., 2007; Hodges et al., 2003, 2011; Wang et al., 2006, 2013). The introduction of satellite observations in 1979 is the prominent example of a discontinuity in the quantity of data for assimilation, which has been the reason for a number of studies to handle data before and after this event separately (Bromwich et al., 2007; Eichler and Gottschalck, 2013a, 2013b; Simmonds et al., 2008). In summary, the types and/or quantity of observations available for assimilation in the reanalysis datasets have changed considerably over time, which could cause discontinuities (sudden changes) in reanalysis data, and in cyclone statistics derived from reanalysis data. For example, Wang et al. (2006) show that ERA40 and NCEP1 have discontinuities in the SH cyclone statistics, which coincide for example with the introduction of satellite data. Wang et al. (2013) show that the 20CR (v2) data contains discontinuities that coincide with the increasing amount of surface pressure observations available for assimilation, although the type of observations assimilated in 20CR does not change over time.

Similar to Wang et al. (2013), we used the RHtestsV4 software package (Wang and Feng, 2013) to assess the temporal homogeneity of cyclone statistics (seasonal counts and intensity) in each reanalysis dataset (the ensemble-averaged statistics for 20CR). We derived the hemispheric/regional mean series of consecutive seasonal cyclone statistics for seven regions: the Arctic (north of 75°N), NH, NH land, NH sea, SH, SH land, and SH sea. We used the PMFred algorithm (Wang, 2008a) in the RHtestsV4 package to check temporal homogeneity of each cyclone statistic time series. The PMFred algorithm is based on the penalized maximal F (PMF) test (Wang, 2008b), which is an improved version of the common trend two-phase regression based test (Wang, 2003) for detecting mean shift without trend change.

The homogeneity tests are conducted at the 5% significance level. The dates/times of major changes in the input data amount and/or types were either used to verify the statistically detected changepoints or tested as potential Type-0 changepoints to assess their statistical significance (see Wang, 2008a). For ERA20C and 20CR, the time series of counts of observations assimilated in the 20CRv2 as shown in Fig. 2 of Wang et al. (2013) was also used to verify the changepoints detected in time series of the ERA20C and 20CR cyclone statistics, because these reanalyses assimilated similar observational data. The changepoints detected in each of the nine datasets are listed in Tables 2 and 3. The time series of cyclone statistics and the regression fits (with changepoints if any) are shown in Figs. S1–S18 in the online Supplementary data.

As shown in Table 2, in terms of all-cyclone statistics, at 5% significance level, ERAint and NCEP2 were found to be homogeneous for both hemispheres (and hence were not listed in Table 2), while MERRA, ERA40, and CFSR were found to be homogeneous for the NH. In terms of deep-cyclone statistics, ERAint, NCEP2, and MERRA were found to be homogeneous for both hemispheres (and hence were not

listed in Table 3); and CFSR and ERA40 were also found to be homogeneous for the NH (Table 3). NCEP1 and JRA55 show discontinuities in both all-cyclone and deep-cyclone statistics for both hemispheres; and so do ERA20C and 20CR (Tables 2–3). JRA55 shows an obvious sudden decrease in the variance of the NH deep-cyclone mean intensity in the end of 1997, and to a lesser extent, in the end of 1972 (see Supplementary Fig. S12 and Table 3). The variance decreases are not obvious in the Arctic (see Supplementary Fig. S12). Just like the 20CRv2 analyzed in Wang et al. (2013), for the NH, version v2c of the 20CR is also homogeneous after 1948 (Tables 2–3 and Figs. S2 and S11).

Most of the changepoints detected (Tables 2 and 3) coincide with changes in input data quantity and/or types. In general, ERA20C was found to be more homogeneous than 20CR (v2 or v2c), especially for the Arctic (see Tables 2–3 and Supplementary Figs. S1–S2 and S10–S11). Also, ERA20C and 20CR have shifts of the opposite signs, especially in the NH (Figs. S1–S2, panels d and f).

The identified changepoints were taken into account in estimating trends in the related time series in this study. Specifically, we fit a common trend multi-phase linear regression to the time series that contains changepoints to estimate the linear trend. The trend estimates are presented and discussed in Section 4.3.2 below. Different datasets cover different periods. For each dataset's whole period of data, the fitted trend lines are shown in Supplementary Figs. S1–S18.

4. Intercomparison of cyclone activity in the nine datasets

4.1. Comparison of cyclone probability distributions

In this section, the nine reanalysis datasets are inter-compared in terms of the distribution of cyclone counts over the core pressure and over the intensity, using the cyclones identified in the common period (1979–2001) of these datasets.

In terms of distribution over the core pressure, MERRA is very different from all the other datasets for the NH (Fig. 1, upper left), showing many more cyclones of shallow-medium (>990 hPa) core pressures than the others. ERAint is similar to CFSR, and so is JRA55 to ERA20C, ERA40 to NCEP1, and NCEP2 to 20CR. ERAint and CFSR have more shallow-medium cyclones than all the other datasets but MERRA. NCEP2 and 20CR have the lowest counts of NH cyclones among the nine datasets. These datasets form two clusters in terms of the NH counts of deep-cyclones (core pressure ≤ 980 hPa), with MERRA, ERAint, CFSR, JRA55, and ERA20C being in a cluster with higher counts of deep-cyclones than the other four datasets (ERA40, NCEP1, NCEP2, 20CR). In the SH (Fig. 1, upper right), the distributions can be divided into two clusters: MERRA, CFSR and ERAint form the cluster of higher cyclone counts, the other six datasets form the cluster of lower cyclone counts. However, in terms of deep-cyclone counts, JRA55 belongs to the cluster of higher cyclone counts.

In terms of distribution over the intensity, CFSR is very different from all the other datasets for both hemispheres (Fig. 1, lower panels), showing many more cyclones of moderate intensity than the others. MERRA is also very different from the others, especially in the NH, where it shows much higher counts of cyclones of intensity ≥30 units ($\times 10^{-5}$ hPa km^{-2}) than the other datasets. JRA55 and ERAint also show more cyclones of intensity ≥30 units than all the other datasets but MERRA.

Here, cyclone intensity is the local Laplacian of pressure, which reflects horizontal pressure gradient, i.e., the geostrophic wind force around the cyclone core. As shown in Fig. 1 (lower panels), MERRA cyclones have stronger geostrophic wind force than cyclones in all the other datasets, including the CFSR, which has a similar horizontal resolution (Table 1). The question arises whether the MERRA cyclones are associated with stronger surface winds than cyclones in the other datasets.

To answer this question, we plot the contour maps of MSLP, surface winds, and 925 hPa winds for all best-match pairs of deep-cyclones in MERRA and CFSR (those that match each other best in the track-to-track comparison described in Section 4.2 below) for winter and summer of 1979 (an arbitrarily chosen seasons). Visual inspection of these maps reveals that, surprisingly, MERRA cyclones are often associated with weaker surface winds than the corresponding CFSR cyclones, while MERRA cyclones have slightly lower core pressure and larger horizontal pressure gradients, as shown in the examples in Fig. 2. In other words, MERRA cyclones tend to have weaker surface wind force but stronger geostrophic wind force (i.e., horizontal pressure gradients) than the corresponding CFSR cyclones. This feature is not seen in the 925 hPa winds, as shown in Supplementary Fig. S19. This must be related to how surface winds were derived in the reanalysis models, including boundary layer parameterization. Note that CFSR used a coupled model, while MERRA used an atmosphere-only 3D-Var analysis system, although the atmospheric analysis system and the input data for CFSR are nearly the same as those used in MERRA (Sahaet al., 2010). A comprehensive inter-comparison of surface wind storms in these reanalysis datasets is being undertaken and the results will be reported in a separate study.

4.2. Cyclone track-to-track comparison

In this study, we also investigated the correspondence between individual cyclone tracks in each pair of reanalysis datasets, using the track-to-track comparison method of Hodges et al. (2003). Each cyclone track identified in one dataset (say Set A) is compared with those identified in another dataset (say Set B) by first finding the tracks in the Set B that overlap in time with the Set A track. If the number of time points that overlap is ≥60% of the mean number of time points in the two tracks, a possible match in time is identified. For the tracks that satisfy the above temporal matching threshold, the mean separation on the unit sphere is computed from those points that overlap in time using the geodesic distance measure (see Hodges et al., 2003 for details). Occasionally there will be more than one track in the Set B that satisfies the temporal matching threshold; the one with the least mean separation distance is taken to be the matching track. A pair of best-match tracks is a pair of matching tracks with the mean separation distance of no more than 2°.

The track-to-track comparison was carried out using the original cyclone tracking results (with no homogenization, no accounting for inhomogeneities). We carried the track-to-track comparison for the common period 1979–2009 of the eight datasets (all except ERA40). The counts of cyclone tracks in the NH and the SH and the track agreement between each pair of datasets are presented in Table 4. The track agreement is expressed in percentage of best-match tracks, relative to the lower count of tracks in the pair of datasets in question. Each of the 56 members in the 20CR ensemble was compared to each of the other datasets; the comparison results were then averaged over the ensemble members.

For each pair of the nine datasets, the track-to-track comparison was also carried out for their common period (in this case, the period for track-to-track comparison varies from one pair of datasets to another); the results are presented in Supplementary Table S1.

In the NH, annually (Table 4a, upper-right triangle), the best track agreement is found between NCEP1 and NCEP2 (60.8%), then between
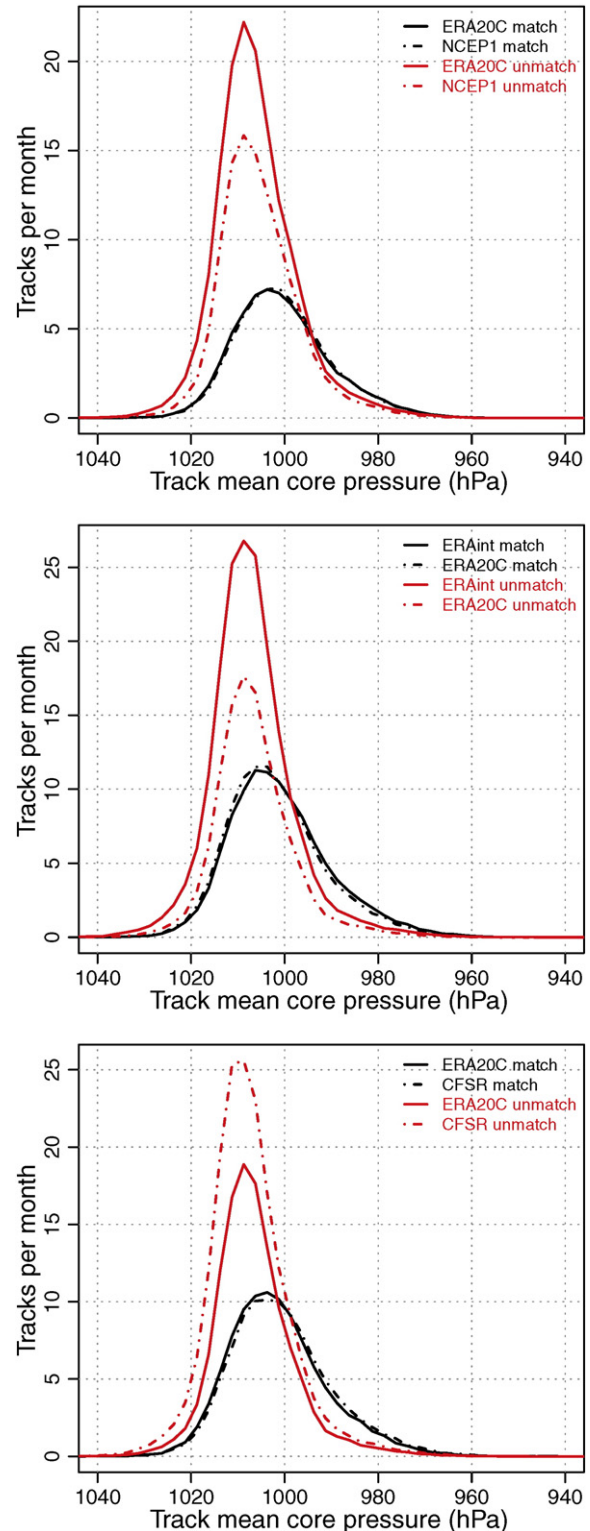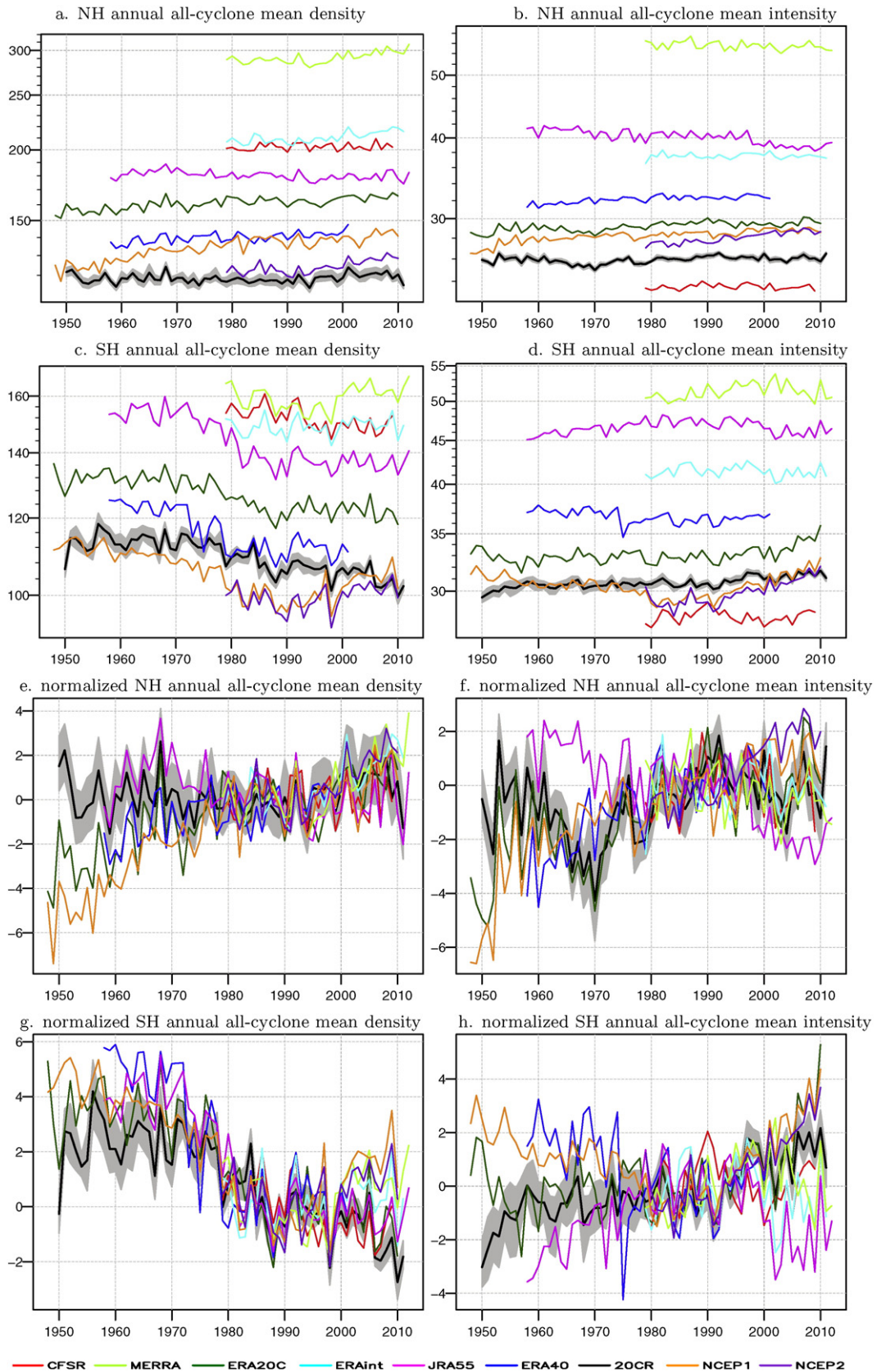

Fig. 3. Distribution of monthly track numbers over the mean core pressure of the best-matched tracks, and of the unmatched tracks in the NH for the indicated datasets.

Fig. 4. Time series of annual all-cyclone mean density (number/count of cyclones per 1,000,000 km^2) and mean intensity (unit: 10^{-5} hPa per km^2) averaged over the indicated hemispheres, as derived from the nine reanalysis datasets. The mean and standard deviation of the period 1979–2001 were used to obtain the normalized time series. The grey-shading indicates the ensemble spread (i.e., the 95% confidence interval) of the 20CR v2c ensemble.
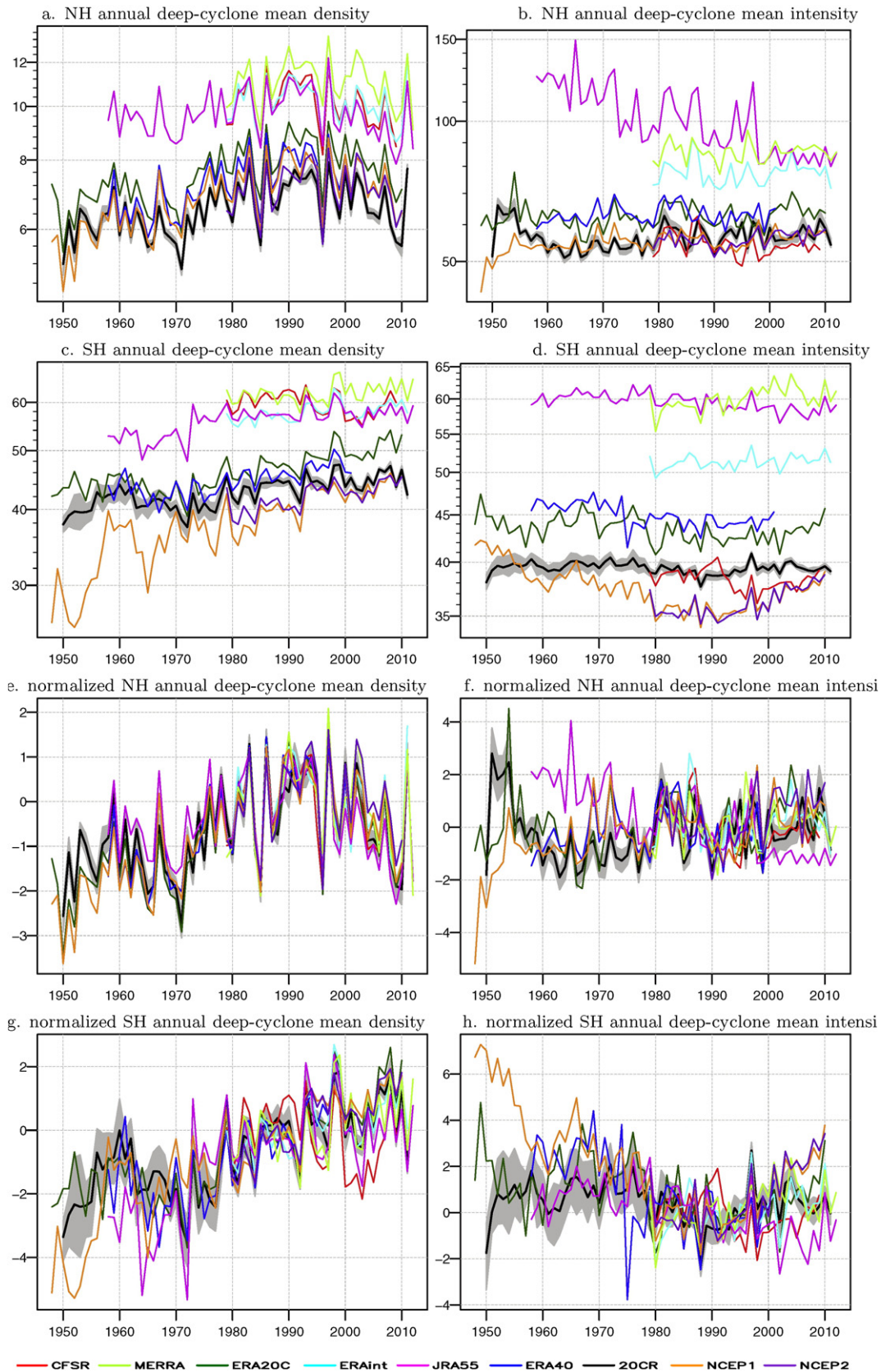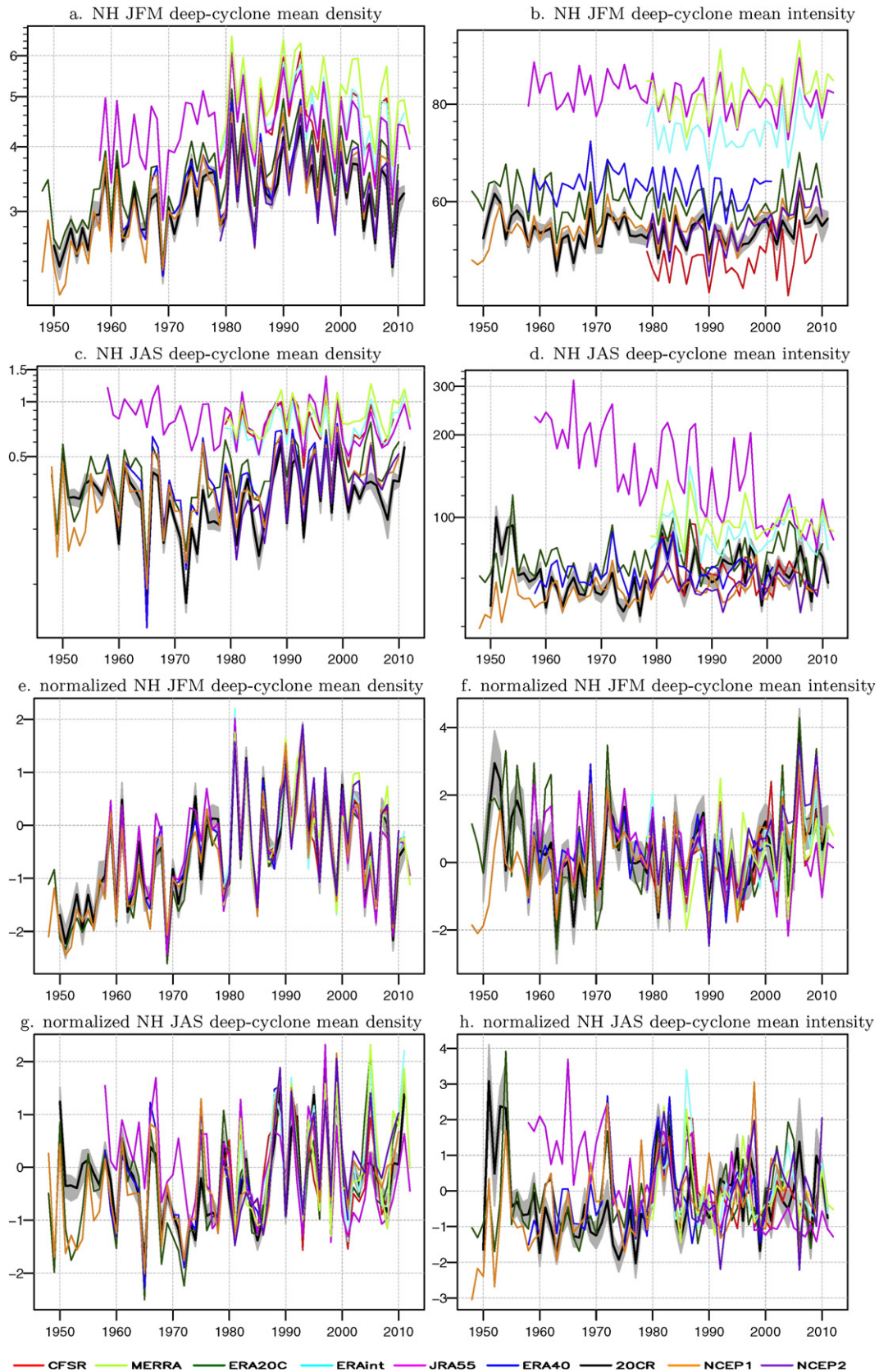
Fig. 5. Same as in Fig. 4 but for the annual deep-cyclone mean density (number/count of deep-cyclones per 1,000,000 km^2) and mean intensity (unit: 10^{-5} hPa per km^2) averaged over the indicated hemispheres.

ERA40 and ERAint (51.4%); ERA40 also has good agreement with NCEP2 (50.8%). The poorest agreement in the NH is found between MERRA and 20CR (29.7%), then between ERAint and 20CR (35.6%).

These features (best or poorest agreement) are generally seen in both seasons, as shown in Table 4b, although the track agreement is generally better in winter (JFM; upper-right triangle) than in
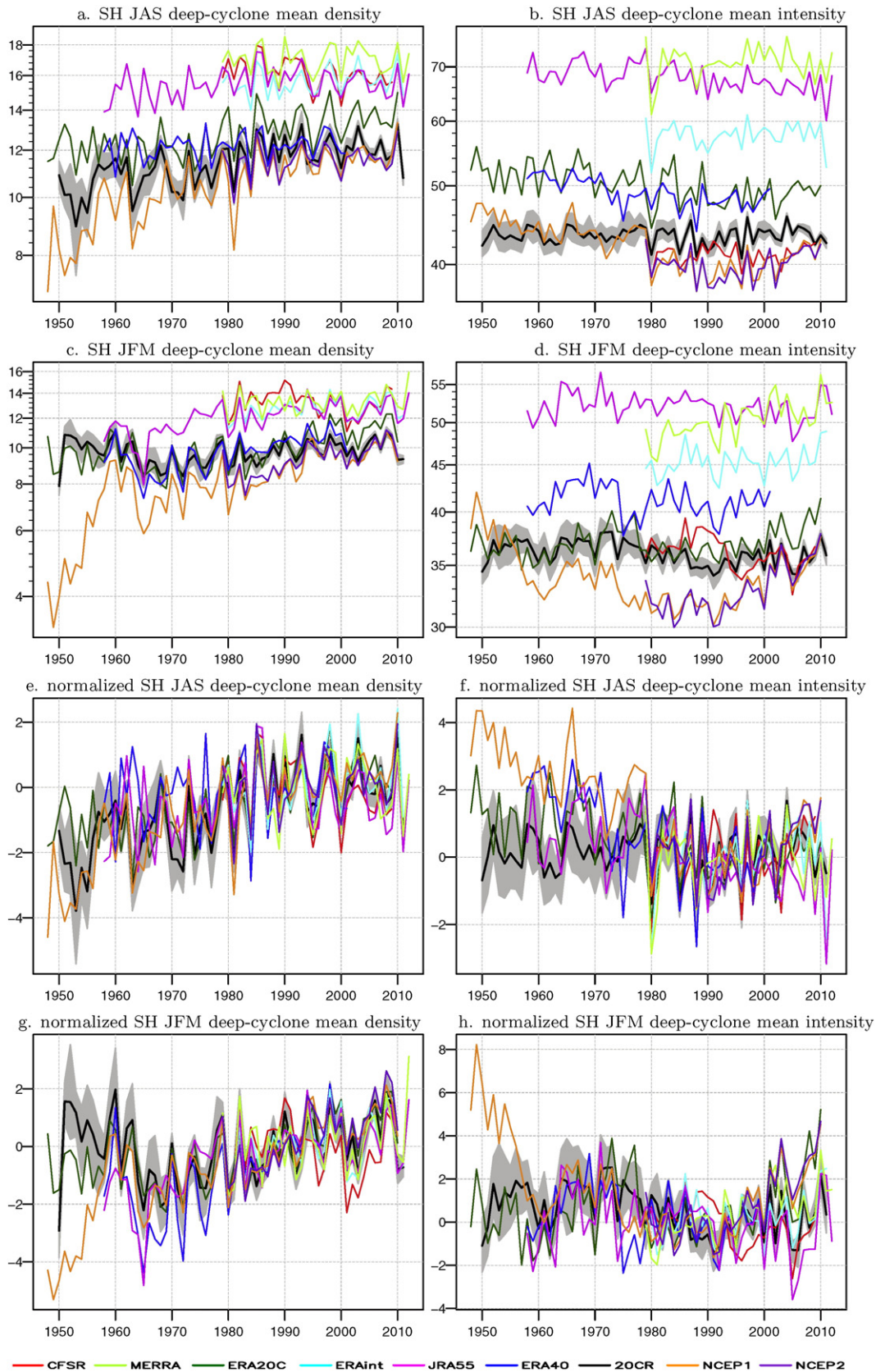
Fig. 6. Same as in Fig. 4 but for the indicated seasonal deep-cyclone mean density (number/count of deep-cyclones per 1,000,000 km^2) and mean intensity (unit: 10^{-5} hPa per km^2) averaged over the NH.

summer (JAS; lower-left triangle). The agreements between ERA20C and the other datasets (Table 4a, row 3) are comparable to those between the other datasets (Table 4a, row 3); while the agreements between 20CR and the other datasets (Table 4a, last column) are a little lower than those between the other datasets, especially in summer (Table 4b, last row).

Fig. 7. Same as in Fig. 4 but for the indicated seasonal deep-cyclone mean density (number/count of deep-cyclones per 1,000,000 km^2) and mean intensity (unit: 10^{-5} hPa per km^2) averaged over the SH.

In the SH, the track agreement is generally not as good as in the NH. Annually (Table 4a, lower-left triangle), the best agreement is found between ERAint and CFSR (46.8%), then between ERAint and ERA40 (46.2%). The poorest agreement in the SH is found between 20CR and ERA20C (8.6%), then between MERRA and ERA20C (9.8%). The agreement between 20CR and ERA20C over the longer period 1900–2010 is

even worse (4.9; see Table S1). The agreements between ERA20C or 20CR and the other datasets are much lower than those between the other datasets in both seasons (Table 4c). These indicate that the century reanalyses for the SH are not well constrained.

As shown in Table 4c, the SH track agreement is slightly better in austral winter (JAS; lower-left triangle) than in austral summer (JFM; upper-right triangle). In austral winter (Table 4c, lower-left triangle), the best agreement is found between ERAint and CFSR (52.3%), then between ERAint and ERA40 (50.8%) and between ERA40 and CFSR (45.5%); while the poorest agreement is between ERA20C and 20CR (8.1%) or ERA20C and MERRA (8.7%). In austral summer (Table 4c, upper-right triangle), the best agreement is between ERA40 and ERAint (42.3%) and between NCEP1 and NCEP2 (42.2%); and the poorest agreement, between ERA20C and 20CR (9.5%) or MERRA (11.0%).

For the pair of the longest datasets, ERA20C and 20CR, we also make a track-to-track comparison for the period 1970–2010, in addition to the periods 1979–2009 and 1900–2010. We found that the track agreement between ERA20C and 20CR is better in the recent period (1970–2010) than in the whole common period since 1900; it increases from 29.3% to 36.3% for the NH, and from 4.9% to 10.5% for the SH. The better agreement between the datasets must be related to the increased quantity of data available for assimilation into the reanalyses in the recent decades (see Fig. 2 of Wang et al., 2013).

In general, the best-match tracks are generally those with a deeper mean core pressure than the unmatched tracks (i.e., all tracks that are not identified as best-match tracks). This is illustrated in the distribution of monthly track numbers over the track-mean core pressure of the best-match tracks, and of the unmatched tracks (a few examples are shown in Fig. 3): the peaks of the black curves (best-match tracks) are generally associated with a lower pressure than the peaks of the corresponding red curves (unmatched tracks). Also, the best-match tracks in one dataset share a similar distribution of monthly track numbers over the track-mean core pressure with the best-match tracks in the other dataset (the two black curves in each panel are nearly identical); particularly, there are more tracks of track-mean core pressure of 970–990 hPa in the best-match group than in the unmatched (Fig. 3).

4.3. Comparison of cyclone trends and interannual variability

4.3.1. Comparison of the original time series of cyclone statistics

First of all, we derived regional-averaged annual and seasonal counts and mean intensity of all-cyclones and of deep-cyclones, which are shown in Figs. 4–7. These time series are the original time series (i.e., unadjusted for any discontinuities). For the 20CR v2c ensemble, the ensemble-averaged cyclone statistics are shown along with the ensemble spread (i.e., the 95% confidence interval).

Table 5
Linear trends (change per 100-year) estimated for the homogenized consecutive seasonal time series of regional-averaged cyclone statistics over the common period of ERA20C and 20CR (1900–2010; see a–b), and their common period with JRA55 and NCEP1 (1958–2010; see c–f). Trends of 5% significance or higher are shown in bold. Here, the mean density is the number/count of cyclones per 1,000,000 km². The unit of intensity is 10^{-5} hPa km^{-2}.

Date set (period)	Region	All-cyclones		Deep-cyclones	
		Mean density	Mean intensity	Mean density	Mean intensity
a. ERA20C (1900–2010)	Arctic	**10.2** (7.7, 12.6)	**2.5** (1.8, 3.3)	**1.3** (0.6, 1.9)	−4.2 (−8.5, 0.2)
	NHland	**2.8** (2.1, 3.4)	**0.9** (0.7, 1.0)	**1.0** (0.9, 1.1)	**6.7** (3.7, 9.7)
	NHsea	**3.9** (3.4, 4.3)	**3.4** (2.9, 3.8)	**1.2** (1.0, 1.3)	**4.3** (1.4, 7.2)
	NH	**3.9** (3.5, 4.3)	**1.5** (1.4, 1.7)	**0.9** (0.8, 1.0)	**5.2** (2.6, 7.7)
	SHland	**−1.3** (−1.5, −1.0)	**0.9** (0.5, 1.2)	**1.4** (1.2, 1.6)	**−4.3** (−5.1, −3.5)
	SHsea	**−8.3** (−9.8, −6.9)	**−0.4** (−0.7, −0.1)	**12.0** (10.5, 13.5)	**−3.1** (−3.8, −2.4)
	SH	**−2.4** (−2.8, −2.0)	−0.0 (−0.3, 0.2)	**3.4** (3.0, 3.7)	**−3.4** (−4.1, −2.7)
b. 20CR (1900–2010)	Arctic	**5.6** (4.1, 7.2)	**1.1** (0.5, 1.6)	0.1 (−0.6, 0.7)	**13.3** (8.7, 17.9)
	NHland	**1.1** (0.6, 1.6)	**−0.3** (−0.5, −0.2)	**0.2** (0.1, 0.2)	1.1 (−0.7, 3.0)
	NHsea	0.3 (−0.1, 0.6)	**0.3** (−0.0, 0.7)	**0.3** (0.1, 0.4)	**2.6** (0.4, 4.7)
	NH	**0.9** (0.6, 1.2)	−0.0 (−0.2, 0.2)	**0.2** (0.1, 0.3)	**2.0** (0.2, 3.9)
	SHland	−0.0 (−0.1, 0.1)	**0.6** (0.4, 0.8)	**1.1** (1.0, 1.3)	**0.5** (0.2, 0.9)
	SHsea	−1.1 (−2.2, 0.1)	**1.4** (1.2, 1.5)	**8.0** (6.9, 9.1)	**1.5** (1.2, 1.7)
	SH	−0.1 (−0.4, 0.1)	**1.1** (0.9, 1.2)	**1.9** (1.6, 2.2)	**1.2** (0.9, 1.5)
c. ERA20C (1958–2010)	Arctic	**14.0** (8.2, 19.7)	**5.1** (2.9, 7.3)	2.0 (−0.4, 4.4)	−2.2 (−15.3, 10.8)
	NHland	**2.6** (0.8, 4.4)	**0.6** (0.1, 1.1)	**1.3** (1.0, 1.6)	6.5 (−1.3, 14.3)
	NHsea	**4.4** (3.3, 5.5)	**3.7** (2.5, 4.9)	**1.0** (0.6, 1.5)	6.0 (−0.3, 12.2)
	NH	**3.5** (2.4, 4.5)	**1.8** (1.2, 2.3)	**0.8** (0.5, 1.2)	**6.4** (0.4, 12.4)
	SHland	**−2.2** (−2.9, −1.5)	**1.3** (0.2, 2.4)	**1.5** (1.0, 2.1)	**−5.5** (−7.6, −3.4)
	SHsea	**−6.8** (−11.0, −2.6)	**1.1** (0.2, 2.0)	**17.3** (13.3, 21.2)	**−4.4** (−6.5, −2.3)
	SH	**−2.7** (−3.7, −1.6)	**1.1** (0.2, 2.0)	**4.4** (3.3, 5.5)	**−4.7** (−6.7, −2.6)
d. 20CR (1958–2010)	Arctic	**5.8** (0.8, 10.7)	**2.6** (1.1, 4.2)	1.4 (−0.3, 3.2)	14.6 (−1.9, 31.1)
	NHland	0.7 (−0.5, 2.0)	**0.5** (0.1, 0.9)	0.2 (−0.1, 0.4)	**10.9** (5.3, 16.5)
	NHsea	**1.4** (0.5, 2.3)	**1.6** (0.6, 2.6)	**0.5** (0.0, 0.9)	**8.1** (2.2, 14.0)
	NH	**1.0** (0.2, 1.9)	**1.0** (0.4, 1.5)	**0.3** (0.0, 0.6)	**9.3** (4.4, 14.2)
	SHland	0.0 (−0.4, 0.5)	**0.9** (0.2, 1.6)	**0.7** (0.2, 1.1)	**1.9** (0.8, 3.1)
	SHsea	**−6.3** (−10.2, −2.4)	**1.8** (1.2, 2.3)	**6.0** (3.0, 9.0)	**2.0** (1.1, 2.9)
	SH	−0.4 (−1.3, 0.4)	**1.4** (0.9, 1.9)	**1.2** (0.4, 2.0)	**2.0** (1.1, 2.9)
e. JRA55 (1958–2010)	Arctic	1.4 (−5.4, 8.2)	1.3 (−1.5, 4.1)	1.3 (−1.7, 4.4)	**−20.4** (−39.2, −1.7)
	NHland	**−2.1** (−3.9, −0.3)	**−1.4** (−2.1, −0.7)	0.1 (−0.3, 0.4)	−11.5 (−32.1, 9.0)
	NHsea	**−1.4** (−2.7, −0.2)	**−5.9** (−8.2, −3.7)	**0.9** (0.4, 1.5)	−0.4 (−23.6, 22.7)
	NH	**−1.8** (−3.0, −0.5)	**−2.7** (−3.7, −1.8)	**0.8** (0.4, 1.2)	−3.7 (−24.6, 17.2)
	SHland	**−3.0** (−3.8, −2.2)	**2.4** (0.7, 4.0)	0.3 (−0.2, 0.9)	**−5.8** (−8.1, −3.5)
	SHsea	**−7.1** (−12.0, −2.3)	**5.1** (3.9, 6.4)	1.3 (−2.5, 5.2)	**−4.4** (−6.3, −2.5)
	SH	**−2.1** (−3.4, −0.8)	**4.9** (3.8, 6.1)	0.5 (−0.5, 1.6)	**−4.7** (−6.6, −2.8)
f. NCEP1 (1958–2010)	Arctic	**6.1** (0.8, 11.5)	**5.3** (3.5, 7.1)	2.0 (−0.2, 4.3)	1.0 (−10.4, 12.5)
	NHland	**7.6** (5.5, 9.7)	**1.2** (0.7, 1.8)	**0.7** (0.4, 1.0)	3.6 (−1.2, 8.5)
	NHsea	**4.7** (3.7, 5.7)	**3.5** (2.6, 4.4)	**1.0** (0.6, 1.5)	**5.6** (0.5, 10.7)
	NH	**6.2** (5.0, 7.4)	**1.9** (1.5, 2.4)	**0.8** (0.5, 1.2)	**5.0** (1.2, 8.9)
	SHland	**−1.6** (−2.3, −0.8)	0.6 (−0.3, 1.6)	**1.9** (1.3, 2.4)	**−8.4** (−10.3, −6.5)
	SHsea	**−10.8** (−15.8, −5.9)	**2.5** (1.4, 3.5)	**17.4** (12.8, 22.1)	**−1.6** (−3.3, 0.0)
	SH	**−3.2** (−4.5, −1.9)	**3.0** (2.1, 3.9)	**4.7** (3.5, 6.0)	−1.0 (−2.6, 0.7)

Generally speaking, reanalyses of higher horizontal resolutions show higher density/counts of cyclones. For the NH (Fig. 4a), MERRA and 20CR show the highest and lowest density of all-cyclones, respectively, with NCEP2 being most similar to 20CR. For the SH (Fig. 4c), MERRA still shows the highest density of all-cyclones in general, while NCEP2 and NCEP1 show the lowest density. These features are also seen in the deep-cyclone density, though the differences among the datasets are much smaller for deep-cyclone density. In particular, MERRA, JRA55, CFSR, and ERAint form a cluster of similar deep-cyclone density and show higher deep-cyclone density than the other datasets (Fig. 5a and c).

In terms of the mean intensity (local Laplacian of MSLP) of cyclones, MERRA and CFSR show the highest and lowest mean intensity of all-cyclones, respectively, with 20CR being of the second lowest mean intensity (Fig. 4b). This is the case for both the NH and the SH, except that NCEP1 and ERA40 show notably lower mean intensities than 20CR during the period 1980–2000 (Fig. 4d). The nine datasets form two clusters of similar mean intensities of deep-cyclones, especially for the NH: JRA55, MERRA, and ERAint are in a cluster with higher mean intensities than the other datasets (Fig. 5c–d).

Note that JRA55 shows an obvious sudden decrease in the variance of the deep-cyclone mean intensity at the end of 1997; it has a much larger variance than the other datasets in the pre-1998 period (Fig. 5b and Supplementary Fig. S12).

In order to better focus the intercomparison on the long-term trend direction and interannual variability, we also normalized the

Table 6
Same as in Table 5 but for the common period 1979–2009 of eight datasets (except ERA40).

Date set (period)	Region	All-cyclones		Deep-cyclones	
		Mean density	Mean intensity	Mean density	Mean intensity
ERA20C (1979–2009)	Arctic	**22.5** (8.9, 36.2)	0.5 (−4.0, 5.0)	1.5 (−3.9, 6.9)	**23.7** (−3.6, 51.1)
	NHland	−0.6 (−4.3, 3.1)	0.1 (−1.0, 1.1)	**1.5** (0.9, 2.2)	8.9 (−9.9, 27.8)
	NHsea	**5.0** (2.4, 7.5)	1.6 (−0.5, 3.8)	0.0 (−1.0, 1.1)	−4.6 (−19.1, 9.9)
	NH	**2.0** (−0.2, 4.3)	0.7 (−0.4, 1.8)	0.1 (−0.7, 0.8)	1.9 (−12.6, 16.5)
	SHland	−0.8 (−2.5, 0.9)	**3.0** (0.8, 5.2)	**1.3** (0.1, 2.5)	−0.5 (−4.8, 3.8)
	SHsea	−7.0 (−16.8, 2.7)	**4.3** (2.5, 6.1)	**20.8** (13.3, 28.4)	2.4 (−1.4, 6.1)
	SH	−2.0 (−4.4, 0.5)	**3.8** (2.1, 5.5)	**4.9** (2.8, 7.0)	1.7 (−2.1, 5.4)
20CR (1979–2009)	Arctic	**12.2** (−0.3, 24.7)	−0.1 (−3.8, 3.5)	1.1 (−3.0, 5.2)	15.0 (−21.8, 51.8)
	NHland	**3.8** (1.2, 6.4)	0.1 (−0.7, 0.9)	−0.4 (−1.0, 0.2)	5.0 (−8.4, 18.5)
	NHsea	**2.9** (1.0, 4.7)	0.9 (−0.9, 2.7)	−0.2 (−1.3, 0.8)	−1.3 (−15.0, 12.4)
	NH	**3.4** (1.7, 5.0)	0.4 (−0.5, 1.3)	−0.3 (−1.0, 0.4)	1.6 (−10.0, 13.2)
	SHland	**1.3** (0.4, 2.3)	**1.9** (0.4, 3.4)	0.1 (−0.9, 1.2)	2.0 (−1.1, 5.1)
	SHsea	−5.1 (−13.3, 3.1)	**2.8** (1.5, 4.1)	**11.3** (5.0, 17.5)	**2.0** (−0.3, 4.2)
	SH	0.1 (−1.7, 2.0)	**2.6** (1.4, 3.8)	**2.2** (0.4, 3.9)	**2.0** (−0.4, 4.4)
JRA55 (1979–2009)	Arctic	6.1 (−11.2, 23.4)	−4.8 (−10.7, 1.1)	−0.0 (−6.8, 6.7)	8.6 (−22.8, 40.0)
	NHland	2.1 (−1.9, 6.0)	−0.9 (−2.2, 0.4)	−0.6 (−1.4, 0.2)	−16.7 (−46.5, 13.1)
	NHsea	**−3.0** (−5.5, −0.5)	−1.2 (−5.7, 3.3)	0.7 (−0.5, 1.8)	−29.6 (−80.2, 21.1)
	NH	−0.3 (−3.0, 2.3)	−0.9 (−2.8, 0.9)	0.6 (−0.3, 1.5)	−25.3 (−66.9, 16.4)
	SHland	−1.1 (−2.7, 0.6)	**−4.5** (−7.6, −1.4)	−0.1 (−1.5, 1.2)	**−8.0** (−12.0, −4.0)
	SHsea	−3.4 (−13.7, 6.9)	**−3.2** (−6.2, −0.2)	3.0 (−5.7, 11.7)	**−9.1** (−13.1, −5.2)
	SH	−0.6 (−3.1, 1.9)	**−3.1** (−5.7, −0.5)	0.5 (−1.8, 2.8)	**−8.8** (−12.4, −5.1)
NCEP1 (1979–2009)	Arctic	**10.9** (−1.7, 23.5)	1.5 (−2.0, 5.0)	1.5 (−3.4, 6.4)	5.5 (−17.0, 27.9)
	NHland	2.7 (−1.7, 7.1)	**2.3** (1.2, 3.4)	0.2 (−0.5, 0.9)	4.7 (−6.1, 15.4)
	NHsea	**4.7** (2.5, 6.9)	**2.1** (0.2, 3.9)	0.2 (−0.8, 1.2)	4.0 (−8.6, 16.6)
	NH	**3.7** (1.0, 6.3)	**2.3** (1.2, 3.3)	0.2 (−0.6, 0.9)	4.4 (−5.1, 14.0)
	SHland	0.8 (−0.9, 2.6)	**7.9** (5.9, 9.8)	**1.7** (0.6, 2.9)	−1.1 (−4.8, 2.5)
	SHsea	−1.2 (−10.8, 8.3)	**7.8** (5.7, 10.0)	**24.5** (16.4, 32.6)	2.8 (−0.7, 6.2)
	SH	0.2 (−2.7, 3.0)	**7.7** (6.0, 9.4)	**5.9** (3.8, 8.1)	2.7 (−0.7, 6.1)
MERRA (1979–2009)	Arctic	9.7 (−19.8, 39.3)	−11.2 (−33.5, 11.0)	0.4 (−7.7, 8.5)	−21.4 (−63.2, 20.4)
	NHland	**14.1** (6.4, 21.9)	**−3.7** (−7.3, −0.2)	−0.0 (−1.0, 0.9)	0.1 (−17.7, 17.9)
	NHsea	**4.5** (1.4, 7.6)	2.6 (−1.3, 6.5)	−0.0 (−1.5, 1.4)	8.7 (−12.0, 29.4)
	NH	**9.5** (4.7, 14.3)	−2.3 (−5.2, 0.6)	−0.0 (−1.1, 1.0)	5.0 (−12.7, 22.6)
	SHland	0.2 (−2.4, 2.8)	5.7 (−2.3, 13.7)	1.2 (−0.7, 3.1)	**13.3** (4.5, 22.1)
	SHsea	**−11.5** (−22.3, −0.7)	**7.2** (4.6, 9.7)	5.7 (−2.3, 13.6)	**8.6** (3.4, 13.8)
	SH	−2.2 (−5.3, 0.9)	**9.0** (5.9, 12.2)	2.0 (−0.6, 4.6)	**10.3** (4.5, 16.0)
CFSR (1979–2009)	Arctic	6.6 (−9.4, 22.6)	−1.6 (−4.7, 1.4)	0.2 (−6.9, 7.3)	4.2 (−10.9, 19.4)
	NHland	2.8 (−1.5, 7.1)	−0.4 (−1.2, 0.5)	−0.2 (−1.1, 0.7)	−6.7 (−19.4, 6.0)
	NHsea	−0.1 (−2.8, 2.5)	1.2 (−0.6, 3.1)	**−1.3** (−2.6, 0.0)	**−14.1** (−29.2, 1.0)
	NH	1.4 (−1.3, 4.0)	0.0 (−0.9, 1.0)	−0.7 (−1.7, 0.3)	**−10.9** (−23.9, 2.0)
	SHland	**−2.0** (−3.5, −0.4)	−0.1 (−1.9, 1.7)	0.1 (−1.3, 1.5)	**4.1** (0.6, 7.7)
	SHsea	**12.1** (0.4, 23.8)	**6.0** (4.0, 8.1)	7.0 (−3.1, 17.2)	**10.5** (7.5, 13.5)
	SH	1.3 (−1.4, 3.9)	**4.4** (2.8, 6.1)	0.7 (−2.1, 3.4)	**8.8** (6.3, 11.4)
ERAint (1979–2009)	Arctic	**16.2** (1.1, 31.4)	−0.9 (−5.8, 4.1)	1.0 (−6.2, 8.2)	**31.7** (−1.1, 64.5)
	NHland	**10.8** (5.5, 16.1)	0.3 (−1.1, 1.8)	−0.2 (−1.1, 0.6)	0.2 (−17.4, 17.9)
	NHsea	**5.1** (2.5, 7.6)	1.1 (−1.9, 4.1)	−0.7 (−2.0, 0.6)	6.1 (−19.8, 31.9)
	NH	**8.1** (4.7, 11.4)	0.5 (−0.9, 2.0)	−0.5 (−1.5, 0.5)	3.1 (−17.1, 23.4)
	SHland	−0.1 (−2.1, 1.8)	0.2 (−2.6, 3.0)	**1.2** (−0.2, 2.5)	2.4 (−2.0, 6.9)
	SHsea	**10.2** (−0.9, 21.4)	−1.9 (−5.1, 1.4)	**11.4** (4.4, 18.4)	**2.9** (−0.6, 6.4)
	SH	1.8 (−1.2, 4.7)	−1.0 (−3.6, 1.7)	**2.9** (0.9, 5.0)	2.7 (−0.8, 6.3)
NCEP2 (1979–2009)	Arctic	**15.3** (3.0, 27.7)	2.7 (−2.4, 7.8)	1.8 (−2.7, 6.3)	1.1 (−31.1, 33.3)
	NHland	**5.5** (1.8, 9.2)	**4.6** (3.5, 5.8)	0.1 (−0.5, 0.8)	**10.6** (−0.9, 22.1)
	NHsea	**7.1** (4.8, 9.4)	**6.4** (4.4, 8.3)	0.3 (−0.7, 1.3)	8.2 (−3.0, 19.4)
	NH	**6.3** (3.9, 8.7)	**5.4** (4.3, 6.5)	0.2 (−0.5, 0.9)	**8.8** (0.2, 17.4)
	SHland	0.6 (−0.8, 2.1)	**6.7** (4.6, 8.9)	**1.3** (0.3, 2.2)	**7.4** (3.6, 11.3)
	SHsea	**12.0** (1.2, 22.7)	**8.6** (6.0, 11.3)	**16.9** (10.5, 23.3)	**9.5** (5.6, 13.3)
	SH	**2.7** (−0.1, 5.6)	**8.0** (5.6, 10.5)	**4.1** (2.4, 5.9)	**8.9** (5.1, 12.7)
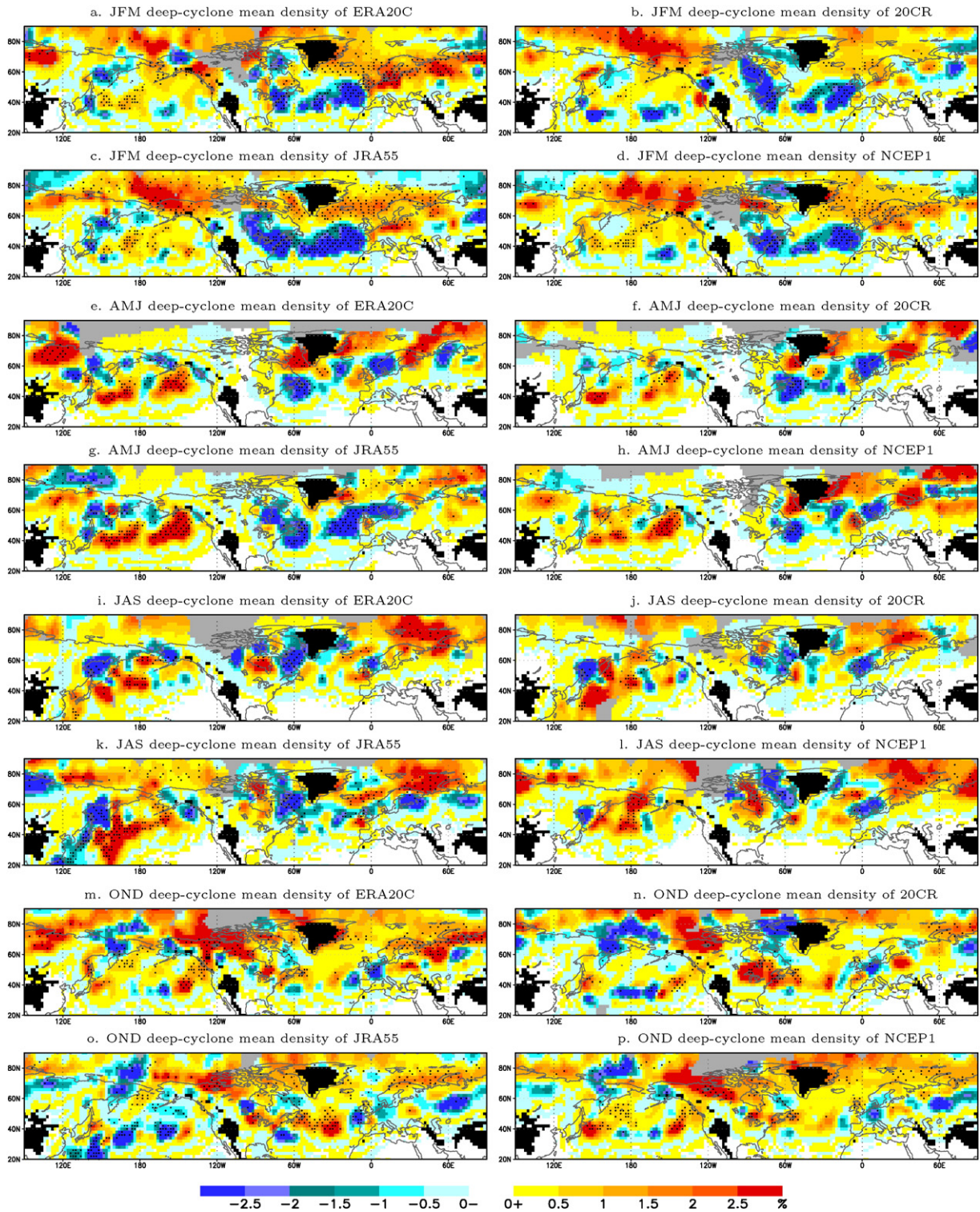
Fig. 8. Maps of linear trends over the period 1958–2010 in the indicated seasonal deep-cyclone counts, as derived from the indicated datasets (homogenized) for the NH. Here, the cyclone statistic is averaged over 750-km grid-boxes, with each 750-km grid-box being centered at a 250-km grid-box. The trends (changes per year) are expressed in percentage of the 1979–2001 climatology of the corresponding cyclone statistic. Stippling indicates areas where the trends are significant at least at 5% level. Elevated areas (elevation > 1500 m) are in black, and areas with no trend estimates are in grey (trend analysis was not performed if the non-zero count of deep-cyclones occurred at this grid-box in <30 years during the 111-year period).

regional-averaged time series of each cyclone statistic, using the mean and standard deviation over the common period 1979–2001. These normalized time series (panels e–h of Figs. 4–7) show clearly how different or similar these datasets are in terms of the long-term trend direction and interannual variability, suppressing the differences in magnitude (which depends partly on the model resolution).

The differences among these datasets are much bigger in the pre-satellite era (before 1979) for both the mean density and intensity of all- and deep-cyclones in both hemispheres. Some of the differences can be related to inhomogeneities in some of the datasets. For example, NCEP1 show much lower all-cyclone density in the NH than the other datasets before 1957 (Fig. 4e); it has a sudden jump in the all-cyclone density in the end of 1956, which was probably due to the fact that

many observational datasets started in 1957 (Kalnay et al., 1996, Appendix A of Uppala et al., 2005). As shown in Fig. 4g, there is also a sudden drop in the end of 1978 in the all-cyclone density in the SH in all the five datasets that have data for the pre-satellite era. This shift is not identified in the NH (Tables 2–3); it is also less obvious for 20CR and ERA20C than for NCEP1, ERA40 and JRA55, which is probably because 20CR and ERA20C did not assimilate satellite data even during the satellite era. All these indicate that the shift in the SH is most likely due to the emergence of satellite data in the late 1970s, which affects the SH much more than the NH, and is less likely linked to the mid-1970s shift in the north Pacific (Trenberth and Hurrell, 1994) or in the whole Pacific climate system (Meehl et al., 2009).

The differences among the datasets are also larger after year 1997, especially for the mean intensity of all-cyclones in the NH and for both the mean density and intensity of all-cyclones in the SH (Fig. 4f–h). Actually, a sudden change in the end of 1997 was identified in the cyclone statistics in both hemispheres in JRA55, and in the SH for MERRA and NCEP1 (Table 2 and Supplementary Figs. S3, S4, S9, S12, S18). This is
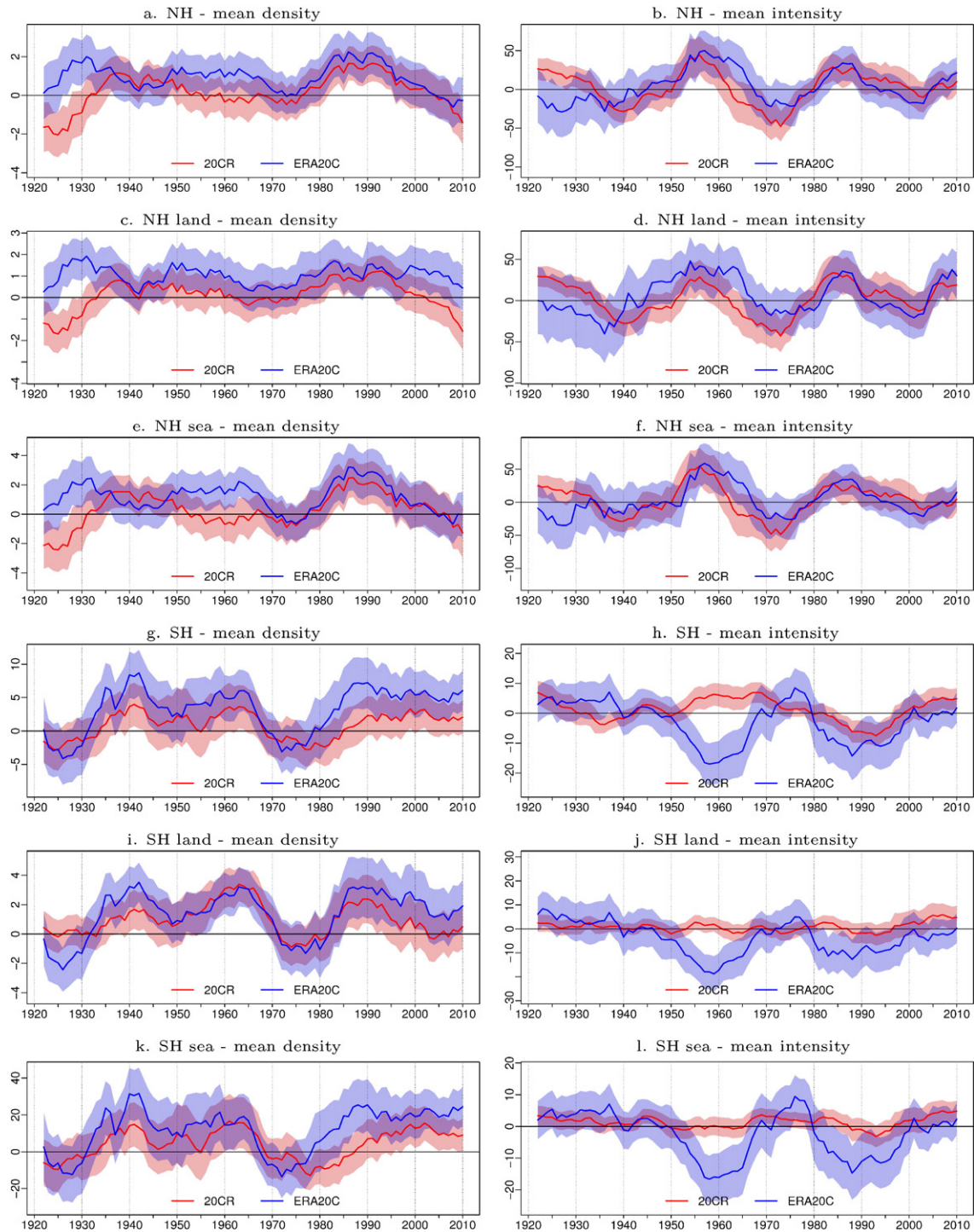
Fig. 9. Linear trends (change per 100-year) estimated from moving 23-year segments of the homogenized time series of deep-cyclone statistics for the indicated regions. The horizontal axis is the last year of the 23-year period. The 95% confidence interval of the trend is shown in shadings. The mean density is the number/count of deep-cyclones per 1,000,000 km². The unit of intensity is 10^{-5} hPa per km².

probably related to changes in the satellite data; for example, AMSU radiances data emerged in 1998 and QuikSCAT marine surface winds data started in 1999 (see Fig. 3 of Rienecker et al., 2011).

As shown in Fig. 5e and g and Table 5, all the four datasets that cover the period 1958–2010 agree well in terms of trend direction and inter-annual variability in hemispheric counts of deep-cyclones, showing a general increase in both hemispheres over the past half century, although the magnitude of increase differs among the datasets. The NH deep-cyclone counts/density peaked around 1960 and 1996, with three lows in 1950, 1971, and 2009; but the lowest counts also show an increasing trend, with the 2009 count being notably higher than the 1950 count. There is inter-decadal variability that is superimposed on the increasing trend.

The agreement in deep-cyclone density is generally better in winter than in summer, and better in the NH than in the SH (Figs. 6–7), with nearly perfect agreement for the normalized density of NH winter cyclones (Fig. 6e). However, the nine datasets do not agree well in terms of trend direction and interannual variability in the deep-cyclone mean intensity, especially in summer and in SH winter (Figs. 6–7, right panels). In particular, NCEP1 shows a sudden decrease in the mean intensity of SH JAS deep cyclones in the end of 1956 and 1978 (Fig. 7f); the 1956 discontinuity is also obvious in mean intensity of SH JFM deep cyclones (Fig. 7h). These datasets agree better on trends when the identified inhomogeneities are accounted for, as discussed next.

4.3.2. Linear trends in homogenized cyclone statistics

In order to account for all the identified discontinuities listed in Tables 2–3, we obtained the linear trend estimates in Tables 5–6 by fitting a multi-phase regression with a common trend throughout the indicated periods. These trend estimates are equivalent to the estimates from the time series that have been adjusted for the identified mean-shifts (also shown in Supplementary Figs. S1–S18). For the datasets and periods shown in Table 5, the linear trends estimated from the original/unhomogenized time series are also presented in Supplementary Table S2 for comparison. The seasonal trends are also estimated from the homogenized data series for each season and presented in Supplementary Tables S3–S10.

4.3.2.1. The 1900–2010 trends in homogenized cyclone statistics. Table 5a–b show the linear trends in the ERA20C and 20CR cyclone statistics over their common period 1900–2010. For the density (number/count of cyclones per 1,000,000 km^2) of all- or deep-cyclones, the homogenized ERA20C and 20CR share the same sign of trends in all the seven regions. Both show a significant (at 5% level) increase in deep-cyclone density in almost all regions in both hemispheres; both also show an increase in the NH all-cyclone density and a decrease in SH all-cyclone density (Table 5a–b). However, 20CR shows generally weaker trends in both all- and deep-cyclone density than does ERA20C; it shows an insignificant trend in the all-cyclone density for NH sea, SH land, and SH, and in the Arctic deep-cyclone density (Table 5a–b). For the Arctic, ERA20C is much more homogeneous (Figs. S1–S2) and hence is probably more reliable than 20CR.

The seasonal trends are less consistent, as shown in Tables S3–S6. Note that the sample size (time series length) for estimating the annual trends (Tables 5–6) is 4 times as large as that for estimating the seasonal trends; so the uncertainty in the annual trend estimates in Tables 5–6 is smaller.

Since all the four datasets that cover the period 1958–2010 show a significant increase in the deep-cyclone density/count over the NH, we derived the maps of the 1958–2010 trends in the NH deep-cyclone density in each season. As shown in Fig. 8, the four datasets show substantial similarity in the NH trend patterns in all seasons. All show increases in the density/count of deep-cyclones over the North Atlantic storm track region and the Barents Sea region in winter, with JRA55 and ERA20C showing more extensively significant increases than 20CR and NCEP1; these were accompanied with significant decreases in the

mid-latitude North Atlantic (Fig. 8a–d). All the four datasets show significant increases in the North Pacific storm track region in spring (Fig. 8e–h), and increases in the Barents Sea region in summer (Fig. 8i–l). In fall, JRA55 shows significant decreases in the region south of Japan, while the other three datasets show no changes in this region (Fig. 8m–p).

More differences between ERA20C and 20CR are seen in the cyclone intensity trends. Both ERA20C and 20CR show an increase in the mean intensity of deep-cyclones over NH land, NH sea, and the NH as a whole, while they show significant trends of the opposite signs in the other regions (Table 5a–b). Also, for NH land, the increase is significant for ERA20C but insignificant for 20CR. For the mean intensity of all-cyclones, they agree on a significant increase for the Arctic, NH sea, and SH land, but they show trends of the opposite signs in the other regions (Table 5a–b).

If the discontinuities in ERA20C and 20CR are ignored (namely, if we fit a single-phase linear regression to the time series), ERA20C and 20CR show significant trends of the opposite signs in both the mean density and intensity of all-cyclones, as well as in the deep-cyclone density, over all the NH regions, and also in the deep-cyclone mean intensity over all the SH regions (see Table S2). The inhomogeneities notably decrease the agreement between the datasets.

In order to show the periods over which the ERA20C and 20CR agree better in linear trends, we estimated linear trends (and their 95% confidence intervals) for moving 23-year segments of the time series of deep-cyclone statistics for the ERA20C and 20CR dataset. As shown in Fig. 9, the best agreements are seen in the NH for both statistics for the period ending 1970 or later (better for the NH sea than for NH land, and slightly better for the density than for the intensity). The poorest agreements are seen in the mean intensity of deep-cyclones over the SH over the periods ending between 1955 and 1965. The 95% confidence intervals of the moving 23-year trends in the two datasets overlap for most of the time in both hemispheres, except for the NH mean density over the periods before 1934 (specially NH land) and for the SH mean intensity over the periods ending between 1955 and 1965 and ending in the early 1980s (Fig. 9). Note that the confidence intervals of the trends are often slightly narrower for 20CR than for ERA20C, due to the fact that the 20CR trends were estimated from the ensemble-averaged cyclone statistics. Also, the 23-year trends fluctuate notably over time in both hemispheres, except for the SH mean intensity of the 20CR deep cyclones (Fig. 9).

4.3.2.2. The 1958–2010 and 1979–2009 trends in homogenized cyclone statistics. Table 5c–f shows the linear trends over the period 1958–2010 for the four datasets that cover this period. All the four datasets consistently show an increase in the density/counts of deep-cyclones in all regions of both hemispheres, although the trend magnitude differs among the datasets (Table 5c–f, column 5). The increase in deep-cyclone density is also discernible in the original time series shown in panels e and g of Figs. 5–7. However, these datasets differ from each other in terms of trend in the deep-cyclone mean intensity: JRA55 shows a decrease but the other three datasets agree on an increase in the NH regions; 20CR shows a significant increase but the other three datasets agree on a decrease for the SH regions (Table 5c–f, last column). For the all-cyclone mean intensity, all the four datasets agree on an increase in the SH, and all but JRA55 also agree on an increase in the NH, with JRA55 showing a decreasing intensity for the NH (Table 5c–f, column 4). More differences are seen among the four datasets in terms of trends in the all-cyclone density, although they agree on an increase in the Arctic region and a significant decrease in SH sea and in SH as a whole. All but JRA55 agree on an increase over the NH, and all but 20CR show a decrease over SH land (Table 5c–f, column 3).

All datasets but ERA40 cover the period 1979–2009. Thus, we compare these eight datasets in terms of the 1979–2009 trends in Table 6. All the eight datasets consistently show an increase in the

all-cyclone density in the Arctic region, and all but MERRA show an increase in the deep-cyclone mean intensity. Except JRA55, all the other seven datasets agree on an increase in the NH all-cyclone density; while all but ERA20C agree on an increase in the all-cyclone density over NH land, and all but JRA55 and CFSR agree on an increase in the all-cyclone density over NH sea (Table 6, column 3). For all-cyclone density over SH land, 20CR shows a significant increase but CFSR shows a significant decrease, while all the other datasets show insignificant changes (Table 6, column 3). For all-cyclone mean intensity, JRA55 shows a decrease in all the seven regions; but NCEP1 and NCEP2 show significant increases in both hemispheres, and are also in agreement with ERA20C and 20CR on an significant increase in all the SH regions (Table 6, column 4). All eight datasets agree on an increase in the deep-cyclone density over SH sea; and all but JRA55 also agree on an increase in the deep-cyclone density over SH land (Table 6, column 5). Despite of the above agreements in the sign of trend, the trend magnitude varies largely among the datasets.

In general, JRA55 is most different from the other seven datasets. It shows a decrease in the mean intensity of deep- or all-cyclones over both hemispheres, while most of the other data sets show either a significant increase or insignificant changes (Table 6, columns 4 and 6).

5. Conclusions

We have intercompared the nine datasets in terms of the climatology, trends and interannual variability of extratropical cyclones. The comparison was done primarily in terms of the cyclone probability distribution and hemispheric/regional-averaged statistics (count and intensity) of cyclones. Time series of the hemispheric/regional-averaged statistics of cyclones were also subject to temporal homogeneity tests. The detected artificial shifts were accounted for in the trend analysis, although the original time series were also intercompared.

In general, the findings of this intercomparison are in agreement with those of the previous studies (e.g., Tilinina et al., 2013). Reanalyses of higher horizontal resolutions show higher cyclone counts, with MERRA and 20CR showing the highest and lowest hemispheric-mean counts/density of all-cyclones, respectively. However, MERRA shows the highest mean intensity of all-cyclones, and CFSR the lowest, although MERRA and CFSR share a similar horizontal resolution. MERRA is the most different from the other datasets, showing many more cyclones of shallow-medium core pressures and much higher counts of cyclones of strong geostrophic winds than the others; while CFSR shows many more cyclones of moderate geostrophic winds than the others. In particular, MERRA cyclones tend to have weaker surface winds but stronger geostrophic winds than the corresponding CFSR cyclones, while the 925 hPa winds are more comparable with each other.

The correspondence between individual cyclone tracks in a pair of datasets (i.e., the track-to-track agreement) is generally better in the NH than in the SH, and better in winter than in summer in both hemispheres. In particular, the best-match tracks are generally those with a deeper track-mean core pressure than the unmatched tracks; and there are more tracks of track-mean core pressure of 970–990 hPa in the best-match group than in the unmatched. In the NH, the agreements between ERA20C and the other datasets are comparable to those between the other datasets; while the agreements between 20CR and the other datasets are a little lower than those between the other datasets, especially in summer. In the SH, the agreements between ERA20C or 20CR and the other datasets are much lower than those between the other datasets in both winter and summer. These indicate that the century reanalyses for the SH are not well constrained.

The differences between the reanalysis datasets are much smaller in the recent decades than in the period before 1979, due to inhomogeneities in some of the datasets in the earlier period. The differences are also much smaller for deep-cyclone counts than for all-cyclone counts. All the four datasets that cover the period 1958–2010 agree well in terms of trend direction and interannual variability in hemispheric counts of deep-cyclones, showing a general increase in both hemispheres over the past half century. However, the trend magnitude varies largely from one dataset to another, which is at least in part due to the resolution differences among the reanalysis models.

The agreement in deep-cyclone counts is generally better in winter than in summer, and better in the NH than in the SH, with nearly perfect agreement for the counts of NH winter deep-cyclones. However, the nine datasets do not agree well in terms of trend and interannual variability in the mean intensity of deep-cyclones, especially in summer and in SH winter.

The results of homogeneity analysis show that ERAint, NCEP2, MERRA, ERA40, and CFSR are homogeneous for the NH, and that ERAint and NCEP2 are also homogeneous for the SH (Tables 2–3). However, large temporal inhomogeneities were found in the other datasets; and most of the identified inhomogeneities coincide with changes in the quantity and/or types of assimilated observational data. These inhomogeneities contribute notably to the differences between the datasets, especially in the earlier period. Better trend agreement between these datasets is seen after the identified inhomogeneities are accounted for. Thus, it is important to identify and account for temporal inhomogeneities before using these reanalysis datasets, especially for trend analysis.

Appendix A. Supplementary data

Supplementary data to this article can be found online at http://dx.doi.org/10.1016/j.atmosres.2016.06.010.

References

Akperov, M.G., Mokhov, I.I., 2010. A comparative analysis of the method of extratropical cyclone identification. Izv. Atmos. Oceanic. Phys. 46, 574–590.

Allen, J.T., Pezza, A.B., Black, M.T., 2010. Explosive cyclogenesis: a global climatology comparing multiple reanalyses. J. Clim. 23, 6468–6484.

Anderson, D., Hodges, K.I., Hoskins, B.J., 2003. Sensitivity of feature-based analysis methods of storm tracks to the form of background field removal. Mon. Weather Rev. 131, 565–573.

Armstrong, R.L., Brodzik, M.J., 1995. An earth-gridded SSM/I data set for cryospheric studies and global change monitoring. Adv. Space Res. 16 (10), 155–163.

Bader, J.M., Mesquita, D.S., Hodges, K.I., Keenlyside, N., Osterhus, S., Miles, M., 2011. A review on Northern Hemisphere sea-ice, storminess and the North Atlantic oscillation: observations and projected changes. Atmos. Res. 101, 809–834.

Bromwich, D.H., Fogt, R.L., Hodges, K.I., Walsh, J.E., 2007. A tropospheric assessment of the ERA-40, NCEP, and JRA-25 global reanalyses in the polar regions. J. Geophys. Res. 112, D10111.

Chang, E., Yau, A., 2016. Northern Hemisphere winter storm track trends since 1959 derived from multiple reanalysis datasets. Clim. Dyn. http://dx.doi.org/10.1007/s00382-015-2911-8 (in press).

Compo, G.P., Whitaker, J.S., Sardeshmukh, P.D., Matsui, N., Allan, R.J., Yin, X., Gleason Jr., B.E., Vose, R.S., Rutledge, G., Bessemoulin, P., Brönnimann, S., Brunet, M., Crouthamel, R.I., Grant, A.N., Groisman, P.Y., Jones, P.D., Kruk, M.C., Kruger, A.C., Marshall, G.J., Maugeri, M., Mok, H.Y., Ã¯, N., TF, R., RM, T., XLL, W., SD, W., SJ, W., 2011. The Twentieth Century Reanalysis Project. Q. J. R. Meteorol. Soc. 137, 1–28. http://dx.doi.org/10.1002/qj.776.

Dee, D.P., et al., 2011. The ERA-interim reanalysis: configuration and performance of the data assimilation system. Q. J. R. Meteorol. Soc. 137 (656), 553–597. http://dx.doi.org/10.1002/gj.828.

Ebita, A., et al., 2011. The Japanese 55-year Reanalysis "JRA-55": an interim report. Sci. Online Lett. Atmos. 7, 149–152. http://dx.doi.org/10.2151/sola.2011-038.

Eichler, T.P., Gottschalck, J., 2013a. Interannual variability of Northern Hemisphere storm tracks in coarse-gridded datasets. Adv. Meteorol. 2013, 545463 (15pp Article ID).

Eichler, T.P., Gottschalck, J., 2013b. A comparison of Southern Hemisphere cyclone track climatology and interannual variability in coarse-gridded reanalyses datasets. Adv. Meteorol. 2013, 891260 (16pp, Article ID).

Geng, Q., Sugi, M., 2001. Variability of the North Atlantic cyclone activity in winter analyzed from NCEP–NCAR reanalysis data. J. Clim. 14, 3863–3873.

Gibson, R., Kallberg, P., Uppala, S., Nomura, A., Hernandez, A., Serrano, E., 1997. ERA description. ECMWF Re-analysis Final Rep. Series. Vol. 1 (71 pp).

Gulev, S.K., Zolina, O., Grigoriev, S., 2001. Extratropical cyclone variability in the Northern Hemisphere winter from the NCEP/NCAR reanalysis data. Clim. Dyn. 17, 795–809.

Hanson, C.E., Palutikof, J.P., Davies, T.D., 2004. Objective cyclone climatologies of the North Atlantic — a comparison between the ECMWF and NCEP reanalyses. Clim. Dyn. 22, 757–769.

Hartmann, D.L., A.M.G. Klein Tank, M. Rusticucci, L.V. Alexander, S. Brnnimann, Y. Charabi, F.J. Dentener, E.J. Dlugokencky, D.R. Easterling, A. Kaplan, B.J. Soden, P.W. Thorne, M. Wild and P.M. Zhai, 2013: Observations: atmosphere and surface. In: Climate Change 2013: The Physical Science Basis. Contribution of Working Group I to the Fifth Assessment Report of the Intergovernmental Panel on Climate Change [Stocker, T.F., D. Qin, G.-K. Plattner, M. Tignor, S.K. Allen, J. Boschung, A. Nauels, Y. Xia, V. Bex and P.M. Midgley (eds.)]. Cambridge University Press, Cambridge, United Kingdom and New York, NY, USA.

Hodges, K.I., Hoskins, B.J., Boyle, J., Thorncroft, C., 2003. A comparison of recent reanalysis datasets using objective feature tracking: storm tracks and tropical easterly waves. Mon. Weather Rev. 131, 2012–2037.

Hodges, K.I., Lee, R.W., Bengtsson, L., 2011. A comparison of extratropical cyclones in recent reanalyses ERA-Interim, NASA MERRA, NCEP CFSR, and JRA-25. J. Clim. 24, 4888–4906. http://dx.doi.org/10.1175/2011JCLI4097.1.

Hoskins, B.J., Hodges, K.I., 2002. New perspectives on the Northern Hemisphere winter storm tracks. J. Atmos. Sci. 59, 1041–1061.

Kalnay, E., Kanamitsu, M., Kistler, R., Collins, W., Deaven, D., Gandin, L., Iredell, M., Saha, S., White, G., Woollen, J., Zhu, Y., Chelliah, M., Ebisuzaki, W., Higgins, W., Janowiak, J., Mo, K.C., Ropelewski, C., Wang, J., Leetmaa, A., Reynolds, R., Jenne, R., Joseph, D., 1996. The NCEP/NCAR 40-year reanalysis project. Bull. Am. Meteorol. Soc. 77, 437–471.

Kanamitsu, M., Ebisuzaki, W., Woollen, J., Yang, S.-K., Hnilo, J.J., Fiorino, M., Potter, G.L., 2002. NCEP-DOE AMIP-II reanalysis (R-2). Bull. Am. Meteorol. Soc. 83, 1631–1643. http://dx.doi.org/10.1175/BAMS-83-11-1631.

Kistler, R., et al., 2001. The NCEP–NCAR 50-year reanalysis: monthly means CD-rom and documentation. Bull. Am. Meteorol. Soc. 82, 247–267.

Kobayashi, S., et al., 2015. The JRA-55 reanalysis: general specificications and basic characteristics. J. meteor. Soc. Japan 93 (1), 5–48. http://dx.doi.org/10.2151/jmsj.2015-001 (in press).

Laprise, R., 1992. The resolution of global spectral models. Bull. Am. Meteorol. Soc. 73 (9), 1453–1454.

Lehmann, A., Getzlaff, K., Harlass, J., 2011. Detailed assessment of climate variability in the Baltic Sea area for the period 1958 to 2009. Clim. Res. 46, 185–196.

Li, M., Woollings, T., Hodges, K., Masato, G., 2014. Extratropical cyclones in a warmer, moister climate: a recent Atlantic analogue. Geophys. Res. Lett. 41, 8594–8601. http://dx.doi.org/10.1002/2014GL062186.

Meehl, G.A., Hu, A., Sander, B., 2009. The mid-1970s climate shift in the Pacific and the relative roles of the forced versus inherent decadal variability. J. Clim. 22, 780–792.

Neu, U., et al., 2013. IMILAST — a community effort to intercompare extratropical cyclone detection and tracking algorithms. Bull. Am. Meteorol. Soc. 94, 529–547.

Onogi, K., et al., 2007. The JRA-25 reanalysis. J. Meteor. Soc. Japan 85, 369–432.

Poli, P., et al., 2013. The data assimilation system and initial performance evaluation of the ECMWF pilot reanalysis of the 20th-century assimilating surface observations only (ERA-20C). ERA Rep. Ser. 14 (62 pp.).

Raible, C.C., Della-Marta, P.M., Schwierz, C., Wernli, H., Blender, R., 2008. Northern hemisphere extratropical cyclones: a comparison of detection and tracking methods and different reanalyses. Mon. Weather Rev. 136, 880–897.

Rienecker, M.M., Suarez, M.J., Gelaro, R., Todling, R., Bacmeister, J., Liu, E., Bosilovich, M.G., Schubert, S.D., Takacs, L, Kim, G.-K., Bloom, S., Chen, J., Collins, D., Conaty, A., da Silva, A., et al., 2011. MERRA: NASA's modern-era retrospective analysis for research and applications. J. Clim. 24, 3624–3648. http://dx.doi.org/10.1175/JCLI-D-11-00015.1.

Saha, S., et al., 2010. The NCEP climate forecast system reanalysis. Bull. Am. Meteorol. Soc. 91, 1015–1057. http://dx.doi.org/10.1175/2010BAMS3001.1.

Serreze, M.C., 1995. Climatological aspects of cyclone development and decay in the Arctic. Atmosphere-Ocean 33, 1–23.

Serreze, M.C., Carse, F., Barry, R.G., Rogers, J.C., 1997. Icelandic low cyclone activity: climatological features, linkages with the NAO, and relationships with recent changes in the Northern Hemisphere circulation. J. Clim. 10 (3), 453–464.

Simmonds, I., Keay, K., 2000. Variability of Southern Hemisphere extratropical cyclone behavior, 1958–97. J. Clim. 13, 550–561.

Simmonds, I., Burke, C., Keay, K., 2008. Arctic climate change as manifest in cyclone behavior. J. Clim. 21, 5777–5796.

Sinclair, M.R., 1994. An objective cyclones climatology for the Southern Hemisphere. Mon. Weather Rev. 122, 2239–2256.

Sinclair, M.R., 1997. Objective identification of cyclones and their circulation intensity, and climatology. Weather Forecast. 12, 595–612.

Tilinina, N., Gulev, S.K., Rudeva, I., Koltermann, P., 2013. Comparing cyclone life cycle characteristics and their interannual variability in different reanalyses. J. Clim. 26, 6419–6438.

Trenberth, K.E., Hurrell, J.W., 1994. Decadal atmosphere-ocean variations in the Pacific. Clim. Dyn. 9, 303–319.

Trigo, I.F., 2006. Climatology and interannual variability of storm-tracks in the Euro-Atlantic sector: a comparison between ERA-40 and NCEP/NCAR reanalyses. Clim. Dyn. 26, 127–143.

Ulbrich, U., Leckebusch, G.C., Pinto, J.G., 2009. Extra-tropical cyclones in the present and future climate: a review. Theor. Appl. Climatol. 96, 117–131. http://dx.doi.org/10.1007/s00704-008-0083-8.

Uppala, S.M., et al., 2005. The ERA-40 re-analysis. Q. J. R. Meteorol. Soc. 131, 2961–3012.

Wang, X.L., 2003. Comments on "Detection of undocumented changepoints: a revision of the two-phase regression model". J. Clim. 16, 3383–3385.

Wang, X.L., 2008a. Accounting for autocorrelation in detecting mean shifts in climate data series using the penalized maximal t or F test. J. Appl. Meteorol. Climatol. 47, 2423–2444. http://dx.doi.org/10.1175/2008JAMC1741.1.

Wang, X.L., 2008b. Penalized maximal F test for detecting undocumented mean shift without trend change. J. Atmos. Ocean. Technol. 25, 368–384. http://dx.doi.org/10.1175/2007/JTECHA982.1.

Wang, X.L., Feng, Y., 2013. RHtestsV4 user manual. Climate Research Division, Science and Technology Branch. Environment Canada, Toronto, Ontario, Canada (29 pp. Available online at http://etccdi.pacificclimate.org/software.shtml published online).

Wang, X.L., Swail, V.R., Zwiers, F.W., 2006. Climatology and changes of extratropical cyclone activity: comparison of ERA-40 with NCEP–NCAR reanalysis for 1958–2001. J. Clim. 19, 3145–3166. http://dx.doi.org/10.1175/JCLI3781.1.

Wang, X.L., Feng, Y., Compo, G.P., Swail, V.R., Zwiers, F.W., Allan, R.J., Sardeshmukh, P.D., 2013. Trends in low frequency variability of extra-tropical cyclone activity in the ensemble of twentieth century reanalysis. Clim. Dyn. 40, 2775–2800.

Wernli, H., Schwierz, C., 2006. Surface cyclones in the ERA-40 data set (1958–2001). Part I: novel identification method and global climatology. J. Atmos. Sci. 63, 2486–2507.

World Meteorological Organization (WMO), 1970. The Beaufort Scale of Wind Force. Reports on Marine Science Affairs No. 3.World Meteorological Organization, Geneva